AURORAL PHENOMENA AT MAWSON, ANTARCTICA.

A thesis for the degree of Master of Science
in the University of Adelaide.

Submitted by:

Brian Patrick Kilfoyle B.A. (Syd)

Mawson Institute for Antarctic Research

December 1969

CONTENTS

ABSTRACT

Using a multichannel photometer with narrow band-pass filters, the intensities of the night sky emissions of $\lambda 5577\text{Å}$ and $\lambda 6300\text{Å}$ of [01], $\lambda 4278\text{Å}$ of N_2^+ and doppler shifted H_β were measured at Mawson, Antarctica.

Plotting the intensities with the time of onset of slowly varying ionospheric absorption events (SVIA) as origin presents an ordered picture which is shown to be consistent with the auroral substorm concept developed by Akasofu. The phenomena accompanying SVIA events are also consistent with the midnight sector poleward bulge phase of the auroral substorm model. Enhanced H_β emission occurred during every SVIA recorded. The simultaneous onset of SVIA events at Mawson, Murmansk and Kiruna on three occasions indicates that SVIA are not localised phenomena.

The distribution of the mantle aurora is found not to lie along the quiet auroral oval, but along lines of constant colatitude. The measured ratios of the intensities of $\lambda 5577\text{Å}$ [01] and $\lambda 6300\text{Å}$ [01] to H_β in proton auroras are much greater than previously reported values.

A procedure for absolute calibration of narrow band-pass filter photometers is outlined.

The derivation of a new geomagnetic "L" co-ordinate system based on McIlwain's "L" parameter is given.

On August 11 and 14 1966 unusual patches of luminosity were observed in the twilight sky. The possibility of their having been aurora or noctilucent clouds is considered, and it is concluded that they were noctilucent clouds at an unusually high altitude.

This thesis contains no material that has been accepted for the award of any degree in any other university and to the best of my knowledge and belief contains no material previously published or written by another person except when due reference has been made in the text.

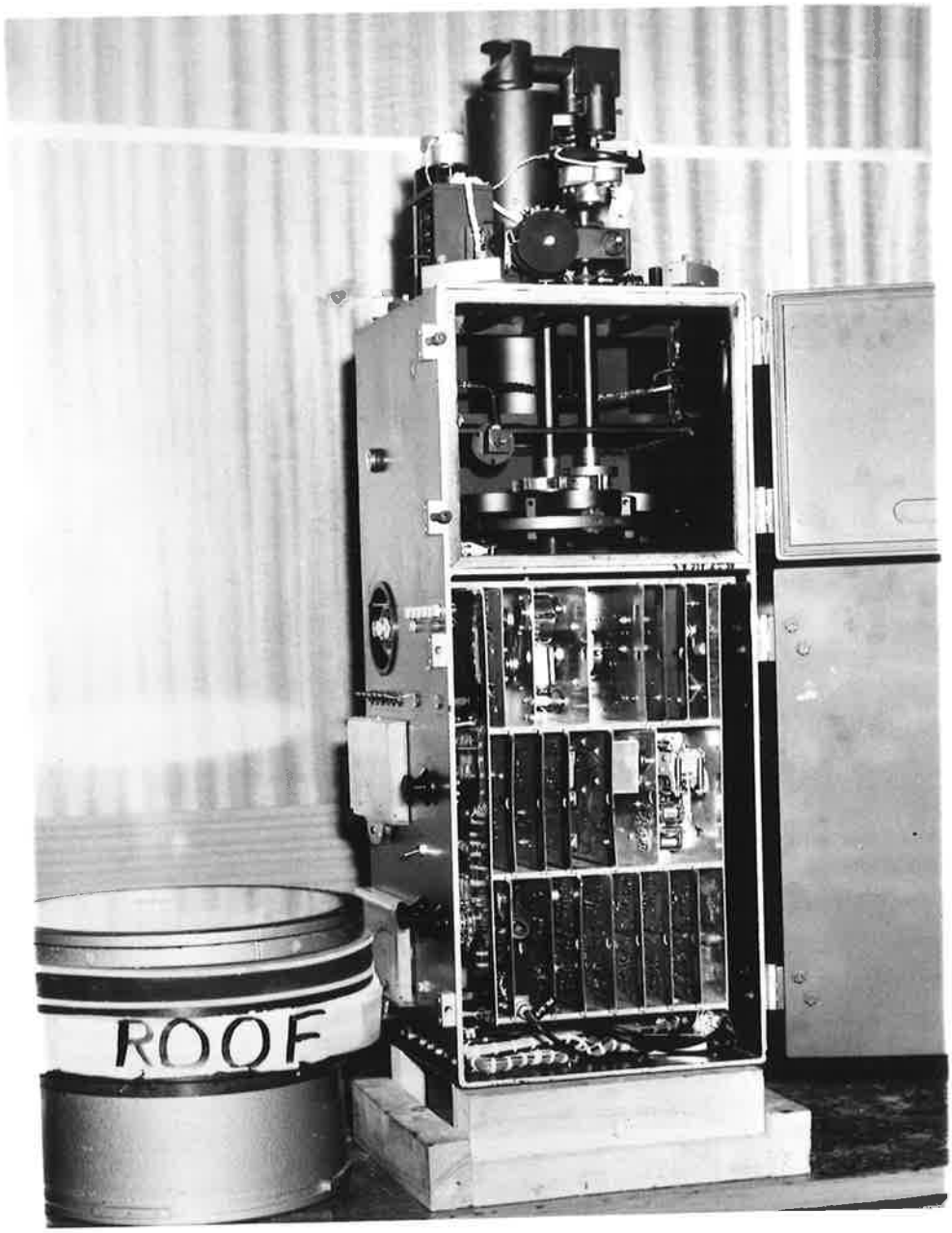

Plate 1. The photometer. The cover glass assembly in the lower left hand corner is fixed into the roof and the photometer is raised into a set orientation in this assembly.

CHAPTER I EQUIPMENT

The photometer, riometer, magnetometer and all sky camera described herein formed part of the total equipment maintained and operated by the author whilst a member of the Australian National Antarctic Research Expedition (ANARE) at Mawson, Antarctica from February 1966 to February 1967. Other equipment operated, the results from which are not applicable to this thesis were an image intensifier and a patrol spectrograph.

Photometer:

The photometer (Plate 1) recorded the intensity in six wavelengths, 4278Å (N_2^+ band emission), 4861Å (H_β), 5300Å (sky background), and 5577Å and 6300Å (atomic oxygen emissions), selected by narrow band pass filters carried in a turret which moved each filter into the optical path sequentially.

Figure 1 is a schematic diagram of the optical components of the photometer and the paths of some light rays through the symmetrical optical system. The maximum angle of acceptance of light at the filter is 2.4°. The bandwidth of the filters as measured in the photometer is 8Å when used with this cone of rays. The field of view is 18°. Light from any point of this field is collimated on to the photocathode, to help overcome problems associated with non-uniformity of the photocathode. (RODMAN and SMITH 1963). The photomultiplier (EMI type 9558B) had a tri-alkali (S20) photocathode.

The photometer circuitry integrates over a period of 50 seconds. The recording system has six ranges automatically selected with an overall full scale deflection ratio of 1024 to 1. Provision is made for continuous mode operation on any one wavelength if desired. A full cycle of the six filters takes six minutes. Once each hour a stable light source is

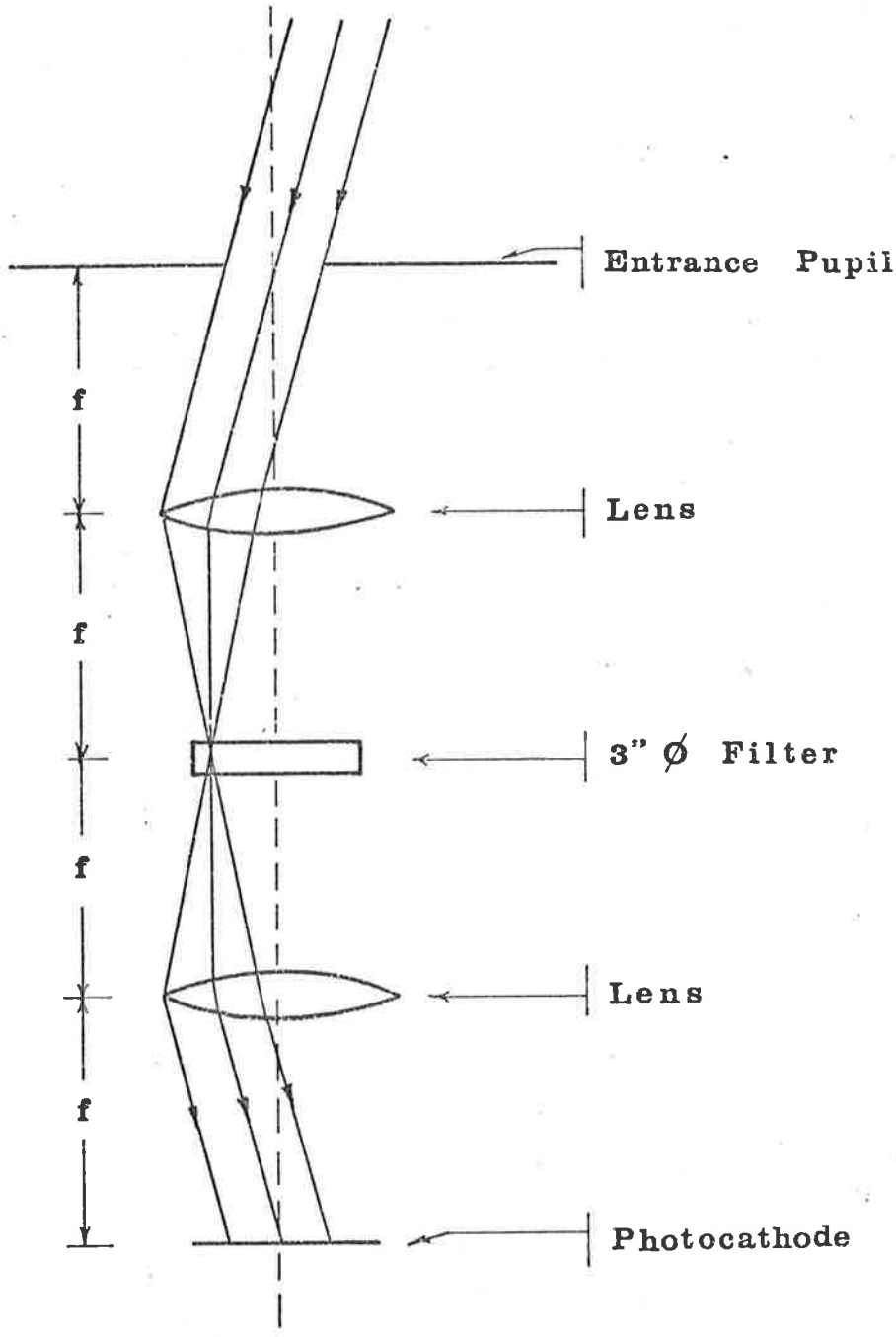

Fig. 1. Schematic diagram of photometer optics.

automatically swung into place over the entrance pupil for a full filter cycle, providing a check on the sensitivity of the photometer. A dark current check is also carried out once per hour to define the zero signal level.

The filters used are multilayer dielectric interference types three inches in diameter. The filter mounts are designed to allow tilting of the filters in the mount for tuning the filters for maximum transmission. A thermostatically controlled electric heating element maintained the filters at a constant temperature to avoid changes in transmission and shifts in peak transmission due to temperature changes.

Calibration of the photometer is carried out by calibrating the inbuilt light source against a tungsten lamp calibrated by the National Standards Laboratory, and measuring the wavelength-transmission profiles of the six filters using a monochromator. (see Chapter II). Hence the photometer is essentially calibrated each hour.

Riometer:

A riometer (LITTLE AND LEINBACH, 1959) monitored the 30 MHz cosmic radio noise continuously throughout the year. The riometer antenna consisted of two $\lambda/2$ dipoles, 0.4 λ apart and 0.15 λ above an earth mat, giving a symmetrical vertical beam of width 64° at the 3 db points, and negligible side lobes. The time constant was 7 seconds, and bandwidth 15 KHz. The riometer was automatically calibrated daily via a noise diode.

Magnetometer:

A horizontal component fluxgate magnetometer designed by the Bureau of Mineral Resources was operated continuously throughout the year.

All Sky Camera:

An all sky camera with a field of view of about 180° and of aperture f/1.0 took one ten second exposure per minute on high speed 35 mm film, on each night of observations. Once each 15 minute cycle one two second and one 40 second exposure was taken.

CHAPTER II PHOTOMETER CALIBRATION

The six channel photometer uses multilayer dielectric interference filters with a band width of about 5Å measured in a collimated beam at normal incidence. The transmission profile $t(\lambda)$ of these filters varies slightly with time and temperature. $t(\lambda)$ also varies with angle of incidence, making it essential that it is measured in the same optical situation in which it is to be used in the photometer. Hence a monochromator must be available to calibrate $t(\lambda)$. To attain sufficient accuracy this necessitates the use of a monochromator of large aperture and good resolution. It is difficult and extremely expensive to maintain such a monochromator at an Antarctic station. A more indirect procedure was devised which makes use of a monochromator with effective aperture f/10 and resolution about 0.5Å at best.

A uniformly illuminated magnesium oxide screen emitting $S(\lambda)$ Rayleigh/Å was set up above the photometer so as to fill the whole field of view. A broad (70Å) band pass filter with transmission coefficient $T_i(\lambda)$, nominally centred on the wavelength λ_i of interest, is placed under the MgO screen (see Figure 2). The narrow band pass filter is removed from the operating position in the photometer. The several rings which locate the filter are replaced in their normal positions so that the aperture presented will be the same as when the filter is in position. A reading $R(S,T_i)$ is taken from the recorder.

We have for each broad band pass filter

$$R(S,T_i) = k \int S(\lambda)\, Q(\lambda)\, X(\lambda)\, T_i(\lambda)\, d\lambda$$

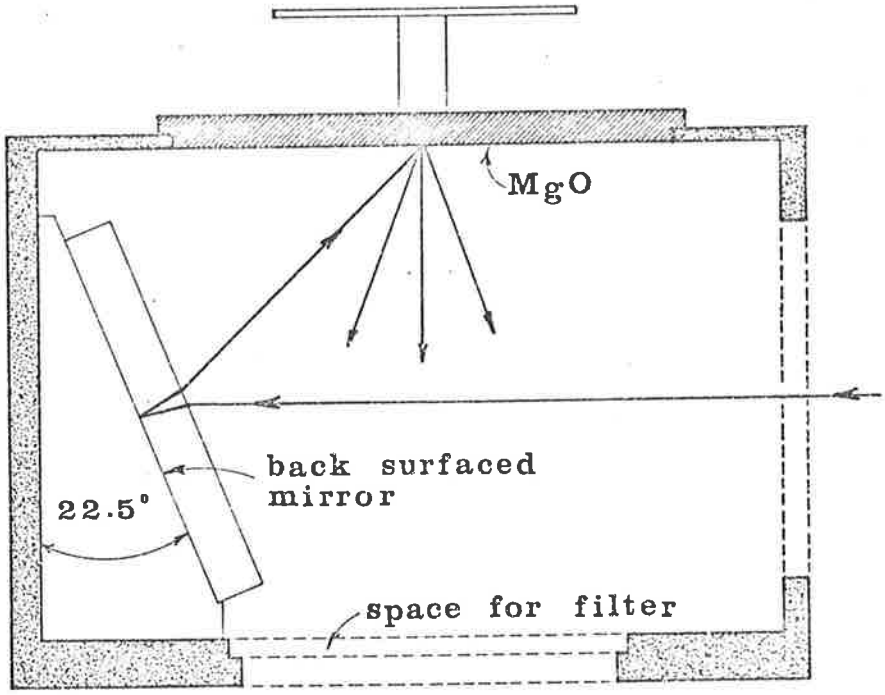

Fig. 2. Detail (not to scale) of the MgO light diffusing box.

where $Q(\lambda)$ is the quantum efficiency of the detector photocathode.

$X(\lambda)$ is the transmission of the photometer optics

k is a constant of the instrument, independant of wavelength,

and the integral is taken over the range of λ for which $T_i(\lambda)$ is significantly non zero.

Examination of the variation of S, Q and X with λ over the range of integration has shown that $S(\lambda)$, $Q(\lambda)$ and $X(\lambda)$ may be taken outside the integral and replaced by their values Q_i, X_i and S_i at the wavelength λ_i of interest without significant error

i.e. $$R(S,T_i) = k\, Q_i\, X_i\, S_i \int T_i(\lambda)\, d\lambda$$

for each of the broad band filters.

Putting $$K_i = k\, Q_i\, X_i$$

we have $$R(S, T_i) = K_i\, S_i \int T_i(\lambda)\, d\lambda \qquad \ldots(1)$$

for each of the broad band filters.

Determination of $\int t_i(\lambda)\, d\lambda$

The broad band pass filter is now removed and the narrow band pass filters replaced. A set of readings $R(S,t_i)$ is taken where

$$R(S, t_i) = K_i\, S_i \int t_i(\lambda)\, d\lambda \qquad \ldots(2)$$

Combining (1) and (2) we get

$$\int t_i(\lambda)\, d\lambda = \frac{R(S,t_i)}{R(S,T_i)} \int T_i(\lambda)\, d\lambda \qquad \ldots(3)$$

Hence, instead of measuring the profile of the narrow band filter $t_i(\lambda)$ and measuring the area under it, we calculate $\int t_i(\lambda)\, d\lambda$ as a function of the profile of the wide band filter $T_i(\lambda)$, which can be measured much more accurately than, and is much more stable with time and temperature than, $t_i(\lambda)$.

The photometer has a stable inbuilt diffuse light source $\Sigma(\lambda)$ Rayleighs/Å that is automatically brought into place over the entrance pupil once each hour, enabling an hourly check on the sensitivity of the photometer to be made. The calibration of the photometer is essentially a calibration of this inbuilt light source.

Determination of Σ_i

Exposing the narrow band filters to S_i we get, as above,

$$R(S,t_i) = K_i S_i \int t_i(\lambda)\, d\lambda \qquad \ldots(4)$$

Exposing these filters to the inbuilt light source, $\Sigma(\lambda)$,

$$R(\Sigma,t_i) = K_i \Sigma_i \int t_i(\lambda)\, d\lambda \qquad \ldots(5)$$

Hence

$$\Sigma_i = \frac{R(\Sigma,t_i)}{R(S,t_i)} \cdot S_i \quad \text{Rayleighs/Å} \qquad \ldots(6)$$

Determination of $\int t_i(\lambda)\, d\lambda, \Sigma_i$ and t_i constitutes a calibration of the photometer.

Application of the Calibration

A line emission of I_i Rayleighs gives a deflection $R(I_i)$ where

$$R(I_i) = K_i I_i t_i \qquad \ldots(7)$$

where t_i is the value of $t_i(\lambda)$ at λ_i.

Each hour the (now calibrated) inbuilt light source Σ_i gives a deflection

$$R(\Sigma_i) = K_i \Sigma_i \int t_i(\lambda)\, d\lambda \qquad \ldots(8)$$

Hence

$$I_i = \frac{R(I_i)}{R(\Sigma_i)} = \frac{\int t_i(\lambda)\, d\lambda}{t_i} \cdot \Sigma_i \qquad \ldots(9)$$

where the RHS of this equation consists of known or measured quantities. Equation (9) is applicable to the [01] oxygen emissions, λ5577Å and λ6300Å only.

To measure the λ4278Å N_2^+ band emission (9) is modified to

$$I_i = \frac{R(I_i)}{R(\Sigma_i)} \cdot \int t_i(\lambda)\, d\lambda \cdot \frac{\int \alpha(\lambda)\, d\lambda}{\int \alpha(\lambda) t_i(\lambda)\, d\lambda} \cdot \Sigma_i \qquad \ldots(10)$$

where $\alpha(\lambda)$ is the profile of the λ4278Å N_2^+ band. Figure 3 is the profile of this band as measured by VEGARD (1932), with low resolution, but adequate for this purpose.

The λ5300Å filter measures the background sky emission, which is fairly flat over the band pass of the filter. Denoting its intensity by A_i Rayleighs/Angstrom we have, when the narrow band filter is exposed to the sky,

$$R(A_i) = K_i A_i \int t_i(\lambda)\, d\lambda$$

When exposed to the inbuilt light source, we have

$$R(\Sigma_i) = K_i \Sigma_i \int t_i(\lambda)\, d\lambda$$

Hence

$$A_i = \frac{R(A_i)}{R(\Sigma_i)} \cdot \Sigma_i \qquad \text{Rayleigh/Å} \qquad \ldots(9)$$

The auroral H_β emission is broadened and when viewed in the zenith is displaced about 6Å to the short wavelength side of normal H_β (4861Å); it is often faint when compared with the background which probably consists mainly of high order molecular band structures. To measure the H_β emission the photometer makes use of two filters which are tuned to 4855Å and 4875Å. It is assumed that the background is similar in the vicinity of these two wavelengths.

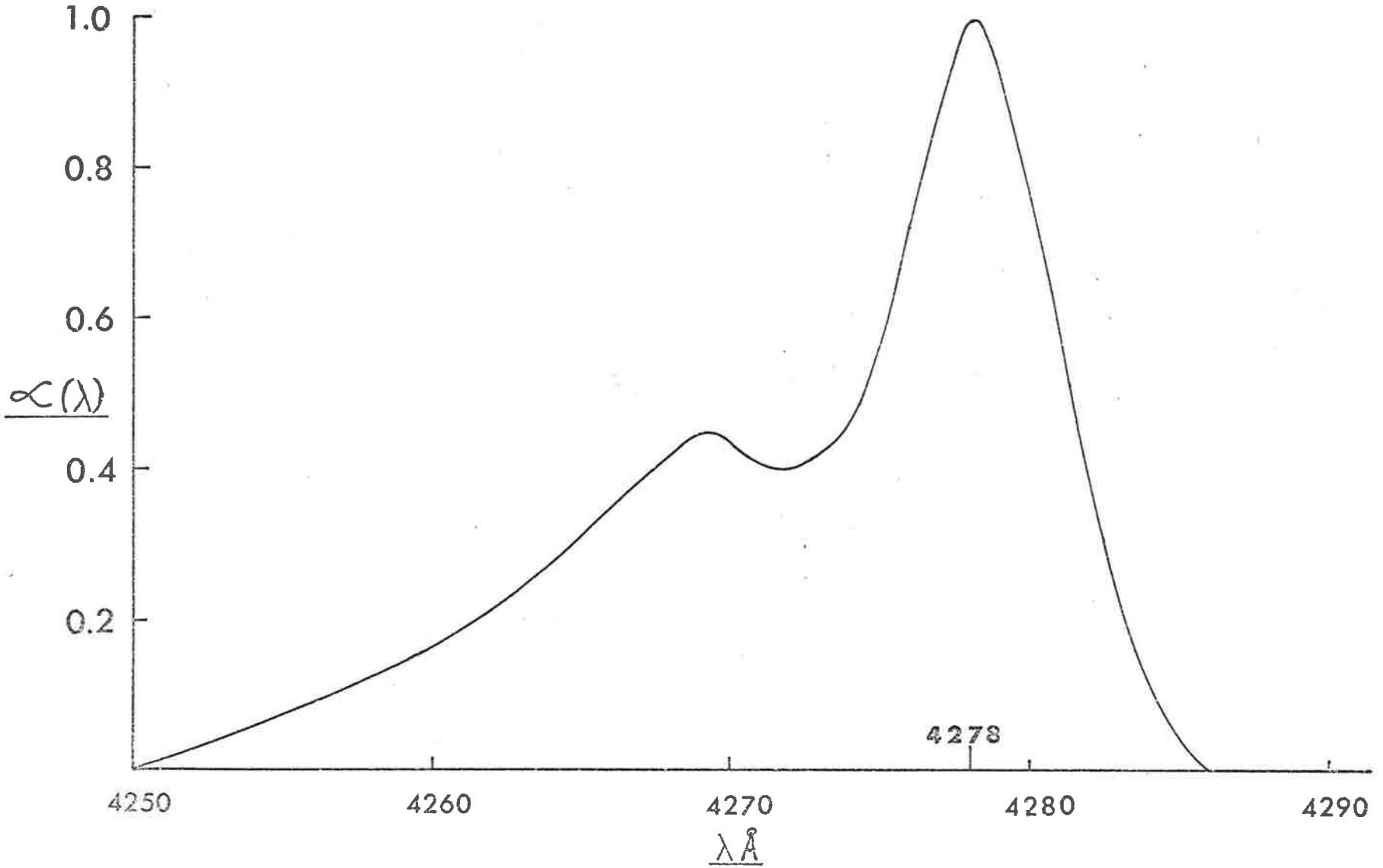

Fig. 3. The normalised λ4278Å N_2^+ band profile α(λ) after VEGARD (1932).

Denoting the background as B Rayleighs/Å and using single primes to denote quantites measured at 4855Å and double primes for those at 4875Å, with the inbuilt light source in position we have,

$$R(\Sigma^o,t') = K^o\Sigma^o \int t'(\lambda)\ d\lambda \qquad ...(12)$$

$$R(\Sigma^o,t'') = K^o\Sigma^o \int t''(\lambda)\ d\lambda \qquad ...(13)$$

where since the wavelength difference is only 20Å, the following approximations have been made,

$$\Sigma^o = \Sigma' = \Sigma''$$

$$K^o = K' = K''$$

when viewing the sky

$$R(B,t'') = K^oB \int t''(\lambda)\ d\lambda \qquad ...(14)$$

$$R(I_\beta,t') = K^oH \int t'(\lambda)_\beta(\lambda)\ d\lambda + K^oB \int t'(\lambda)\ d\lambda \qquad ...(15)$$

where $\beta(\lambda)$ is the profile of the H_β emission normalised to unity at the profile peak and H is the intensity in Rayleighs/Å at the peak; i.e. the total H_β emission I_β is

$$I_\beta = H \int \beta(\lambda)\ d\lambda$$

From (13) and (14)

$$B = \frac{R(B,t'')}{R(\Sigma^o,t'')} \cdot \Sigma^o \qquad \text{Rayleighs/Å} \qquad ...(16)$$

From (12), (15), (16),

$$H = \Sigma^o \cdot \frac{\int t'(\lambda)\ d\lambda}{\int \beta(\lambda)t'(\lambda)\ d\lambda} \cdot \frac{R(I_\beta,t')}{R(\Sigma^o,t')} \cdot \frac{R(B,t'')}{R(\Sigma^o t'')} \qquad \text{Rayleighs/Å} \qquad ...(17)$$

The total H_β emission is

$$I_\beta = \Sigma^o \cdot \frac{\int t'(\lambda)\ d\lambda \cdot \int \beta(\lambda)\ d\lambda}{\int \beta(\lambda)t'(\lambda)\ d\lambda} \cdot \frac{R(B,t'')}{R(\Sigma^o,t'')} \qquad \text{Rayleighs} \qquad ...(18)$$

EATHER and JACKA (1966) examined the published curves for $\beta(\lambda)$ and concluded that that of VEISSBERG (1962) for the magnetic zenith direction was the most consistent with their observations from Mawson. Their observations showed that, in the magnetic zenith direction, the peak of the H_β line profile is displaced $\Delta\lambda = 6 \pm 1$ Å to the short wavelength side of normal H_β (4861Å). Veissberg's line profile, adjusted slightly to make $\Delta\lambda = 6$Å and extrapolated on the long wavelength side was used to define $\beta(\lambda)$ for Mawson (Figure 4).

Measurement of H_β will be contaminated by the presence of narrow profile unshifted H_β from the Milky Way at 4861Å. Correction for this involves reducing I_β in equation (18) by an amount ΔI_β where

$$\Delta I_\beta = \frac{Mt'(4861) \int \beta(\lambda)\, d\lambda}{\int \beta(\lambda) t'(\lambda)\, d\lambda} \quad \text{Rayleighs} \quad \ldots(19)$$

where M is the intensity of H_β from the Milky Way, (MONTBRIAND et al 1955) and t'(4861) is the transmission coefficient of the filter at 4861Å when tuned for maximum transmission at 4855Å.

However, determination of the intensities of the λ4278Å N_2^+ and H_β emissions require a knowledge of the profile of the corresponding narrow band filters. There is no way around this difficulty.

The uniformly illuminated MgO screen was obtained by placing the MgO box as shown in Figure 2 at the entrance pupil of the photometer, with the MgO screen carefully centred on the optical axis.

A calibrated tungsten filament lamp is placed r cm away from the screen. If the radiant intensity of the lamp is $\mathcal{I}(\lambda)$ photons per second per angstrom per steradian, an element of area δA on the MgO screen receives

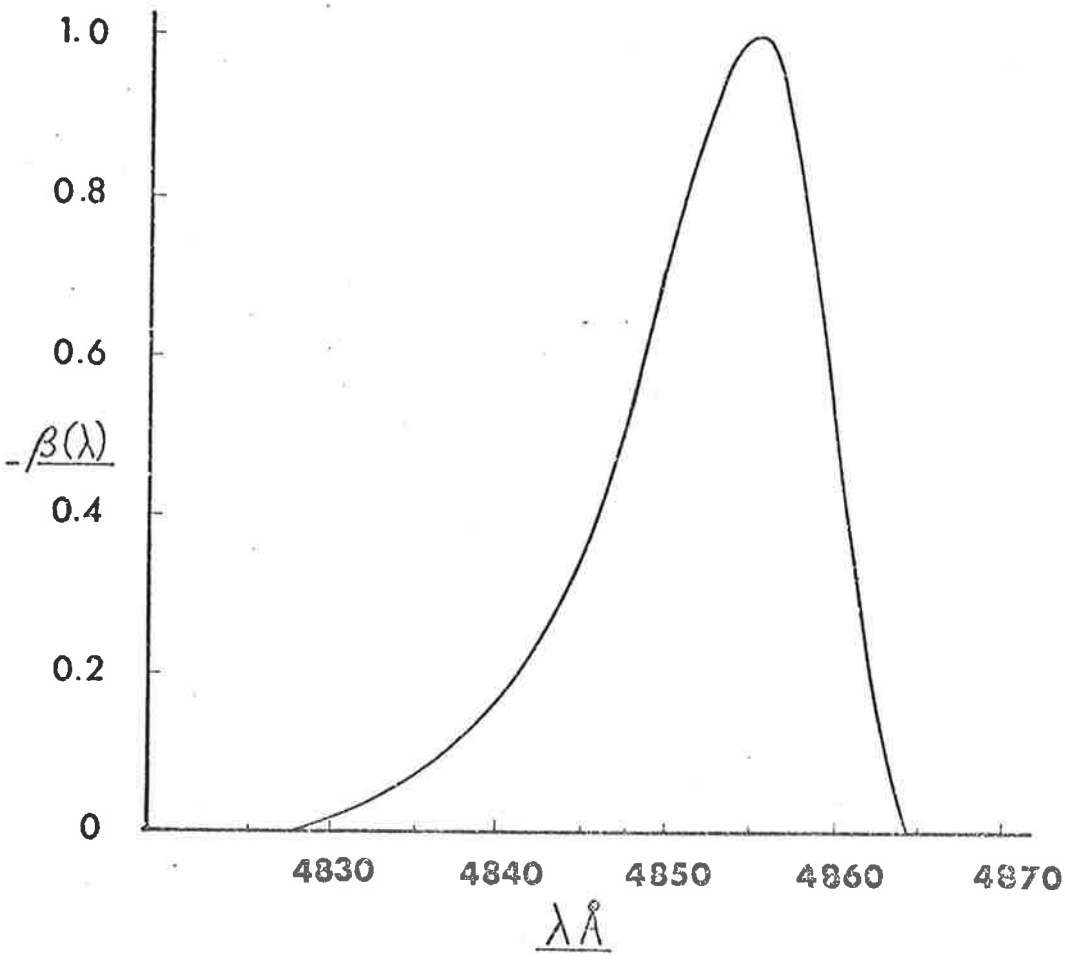

Fig. 4. The normalised H_β profile $\beta(\lambda)$ after EATHER and JACKA (1966b).

$$\frac{I(\lambda)\ \delta A E_1 \cos 45^\circ}{r^2} \qquad \text{photons sec}^{-1}\ \text{Å}^{-1}$$

and scatters

$$\frac{I(\lambda)\delta A E_1 E_2 \cos 45^\circ}{2\pi r^2} \qquad \text{photons sec}^{-1}\ \text{Å}^{-1}\ \text{sterad}^{-1}$$

where E_1 is the specular reflectance of the mirror and E_2 is the diffuse reflectance of the MgO screen. Over the visible range E_1 was measured as 0.87 ± 0.01 and E_2 = 0.98 ± 0.01 (MIDDLETON and SANDERS 1951, GORDON-SMITH 1952). The distance r varies with position of δA on the screen but if r >500 cm the luminance of the screen varies by less than 1% over its area.

The surface luminance of the screen is

$$\frac{I(\lambda)E_1E_2\ \cos 45^\circ}{2\pi r^2} \cdot \frac{4\pi}{10^6} \qquad \text{Rayleigh/Å}$$

or

$$S(\lambda) = \frac{10^{-6}\sqrt{2}\ E_1E_2\ I(\lambda)}{r^2} \qquad \text{Rayleigh/Å} \qquad \ldots(20)$$

Measurement of Filter Parameters

As the transmission of the filters changes with the angle of incidence of the light beam, it is necessary to measure the filter parameters in the optical position in which they will be used. The filters should also be tuned to the correct wavelength before the parameters are measured.

The MgO box was placed on the top of the photometer entrance pupil with a light tunnel from the monochromator exit slit to the box. A tungsten filament lamp was focussed on to the entrance slit. The slit width was chosen as small as feasible consistent with the need for sufficient light output for reliable readings. The photometer itself was used as the detector.

The transmission at a particular wavelength was calculated by measuring the signal with the filter and without the filter in position. The ratio of these readings is the transmission at that wavelength.

The monochromator wavelength scale was checked against various spectral lines from a Cadmium Mercury Zinc discharge lamp.

CHAPTER III GEOMAGNETIC "L" CO-ORDINATES

Geomagnetically associated phenomena when referred to a co-ordinate system related to the configuration of the geomagnetic field exhibit better order than when referred to geographic co-ordinates. Of the several geomagnetic co-ordinate systems in existence (COLE 1963, SIMINOW 1963, HAKURA 1965, HULTQVIST 1958, VEGARD 1912, etc.), the (B,L) system of McILWAIN (1961) has proved most useful for ordering data in latitude.

A system of geomagnetic co-ordinates based on the actual configuration of the mean quiet geomagnetic field is described below. The purpose of this co-ordinate system is the ordering of geophysical data especially at auroral latitudes. The invariant latitude λ defined by $L \cos^2 \lambda = 1$ (where L is the parameter introduced by McIlwain) is used. Longitude and time are defined in the following way.

A line from the centre of the Earth O (Figure 5) to the Sun (at zero declination) at a particular instant cuts through an infinite set of field lines at A_o, B_o, C_o ... and cuts the Earth's surface at P, which lies on the geographic equator. The field lines cut at A_o, B_o, C_o ... intersect the 100 km level at points A_N, B_N, C_N, ... in the northern hemisphere and their conjugates A_S, B_S, C_S ... in the southern hemisphere. The line joining N_L (the north L pole), A_N, B_N, C_N ..., P, ..., C_S, B_S, A_S, and S_L (the south L pole) is defined as a line of L longitude. The L meridian passing through P is labelled with the same numerical value as the geographic meridian passing through P.

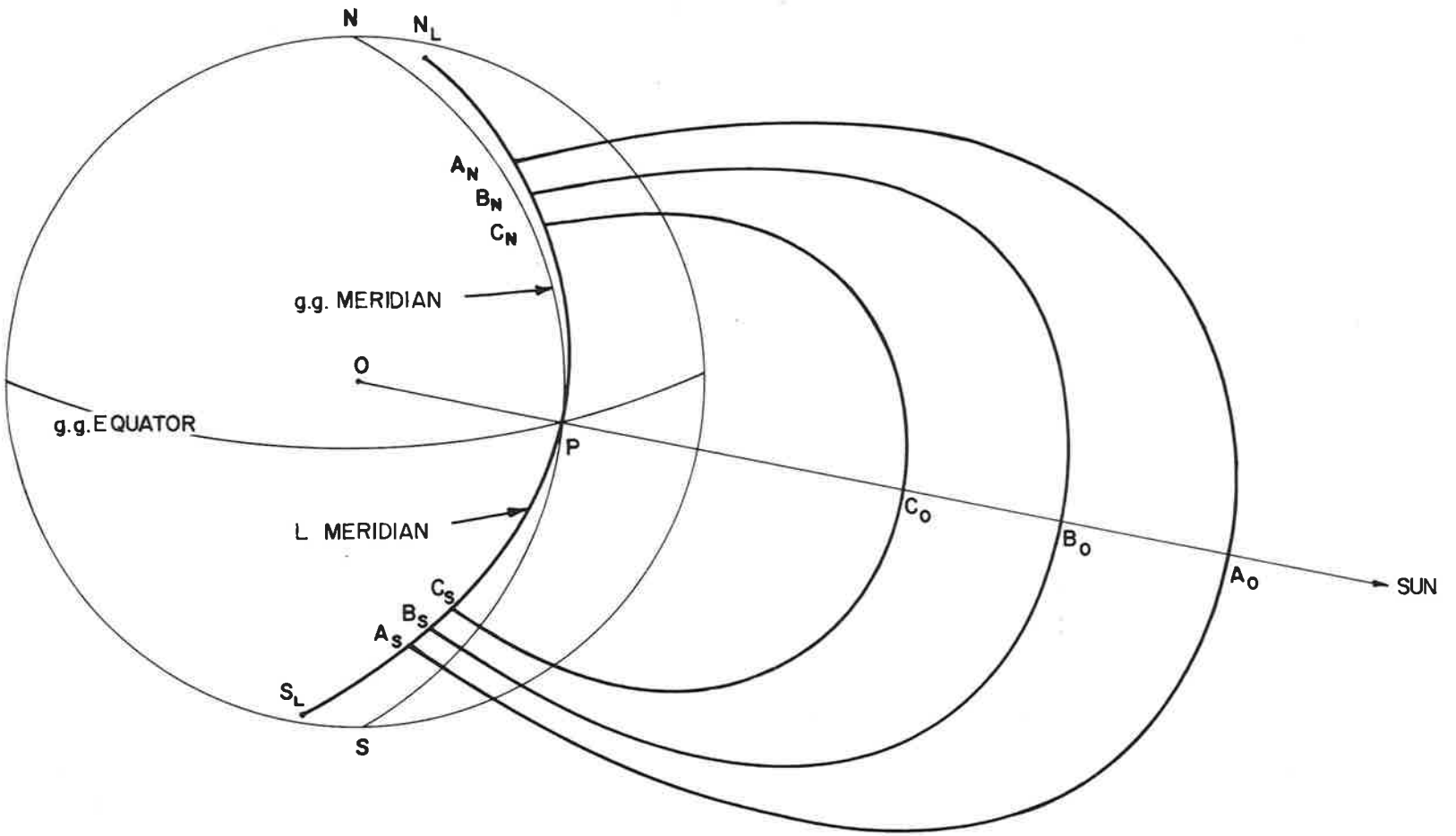

Fig. 5. Schematic diagram indicating the derivation of an L meridian. N and S are the north and south geographic poles and N_L and S_L are the north and south L poles.

The mean L time is defined as being the same at all points on an L meridian, and equal to the mean solar time on the geographic meridian with the same numerical label.

It is assumed here that the important physical processes involved in the interaction of the solar wind with the geomagnetic field occur at low latitudes in the magnetosphere. The upper atmosphere manifestations of this interaction are assumed to be linked with the magnetosphere through the lines of force of the geomagnetic field.

Instead of the centre of the Earth and the geographic equator, the position of the eccentric dipole and the plane of best fit to the L equator could be used; or the intersection of a line joining the L poles and the equatorial plane, and the L equator, and so on. These differ little in their final presentation from that used here, however, which it is believed is the simplest approach and involves negligible concomitant loss of usefulness.

The changing declination of the Sun has not been allowed for, although in principle this could be done, but it is doubtful whether significantly better ordering of data would be achieved.

This L co-ordinate system has the following advantages: (1) it is based on the actual field and not on a dipole approximation to it; (2) conjugate points have the same co-ordinates; (3) the longitudes are rationally labelled; (4) time-longitude equivalence is achieved in the L system as in the geographic system.

The latitude used here has been referred to in the literature as the "invariant" latitude. It is felt that "L" is a better name: it indicates the derivation of the system as well as does "invariant" but

avoids the confusion that can arise through the intrinsic meaning of the word "invariant".

This proposal incorporates some ideas put forward by HULTQVIST (1958), HAKURA (1965) and BOND (1968), but it is felt that this formulation is inherently simpler.

Figures 6 and 7 are polar equidistant geographic grids (light lines) with the geomagnetic L grids (heavy lines) superimposed. These grids were interpolated from data published by HAKURA (1965) and CAMPBELL and MATSUSHITA (1967). The accuracy is believed to be within 2° of great circle arc which is adequate for the present investigation. More accurate grids could have been prepared by considerable computation from the latest field representation, and McIlwains "L" computer program. However, this is an expensive exercise which seemed unwarranted for the purposes of this study.

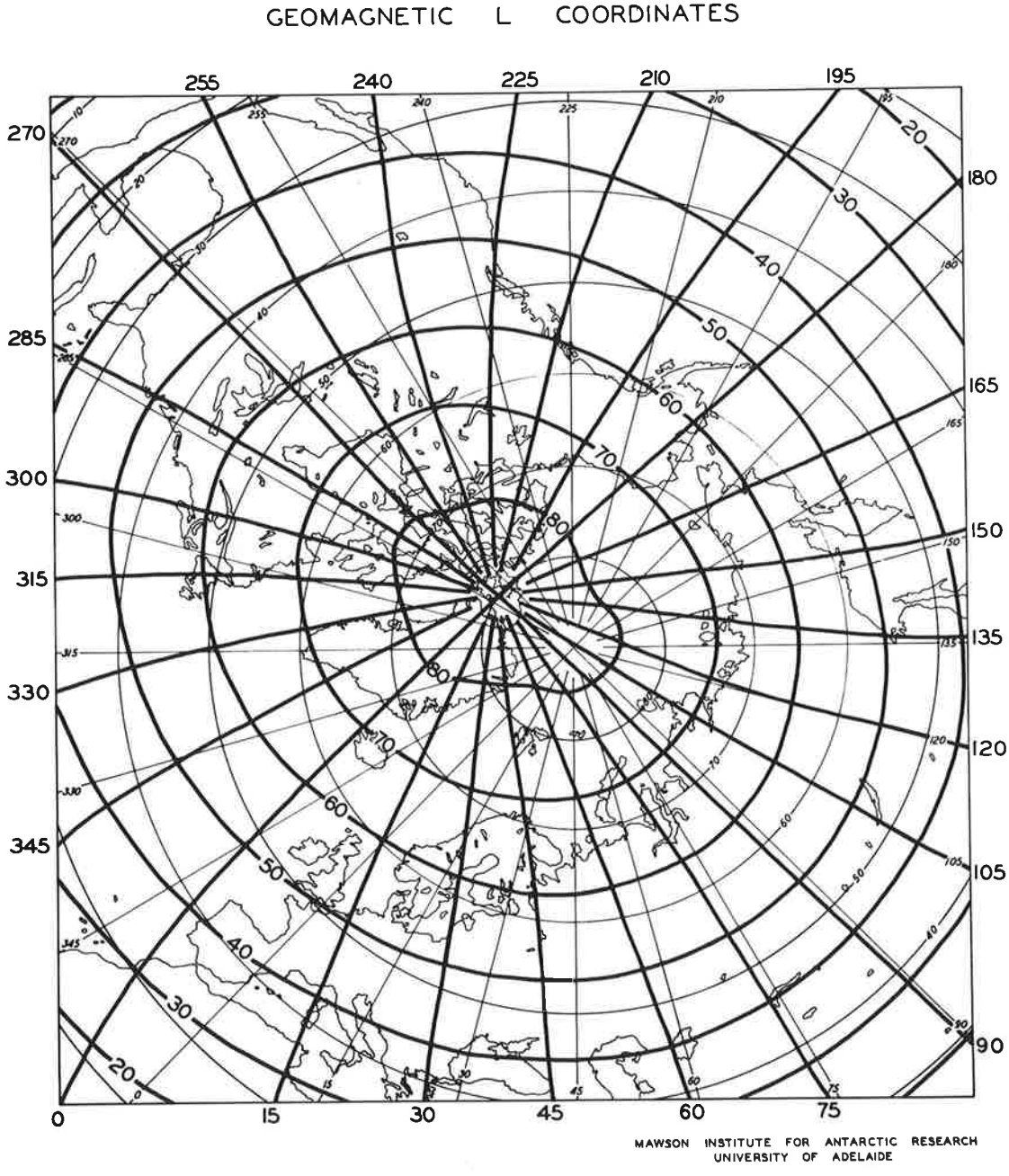

Fig. 6. Polar equidistant geographic projection (light lines) of the northern hemisphere with the L coordinates (heavy lines) superimposed.

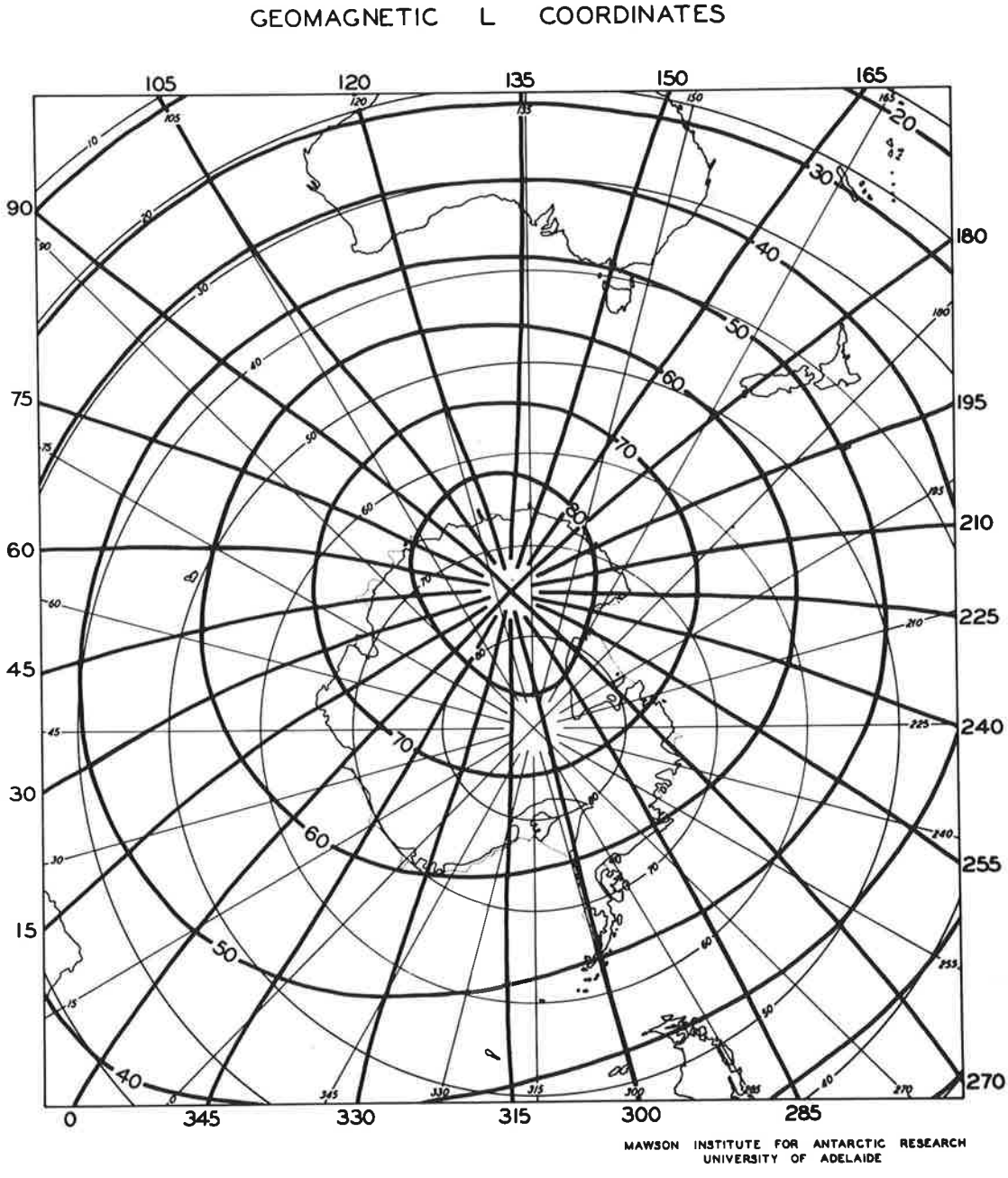

Fig. 7. Polar equidistant geographic projection (light lines) of the southern hemisphere with the L coordinates (heavy lines) superimposed.

CHAPTER IV PHOTOMETER AND RIOMETER RESULTS

(a) BRIEF DESCRIPTION

Half hourly averages of the intensity in Rayleighs of the four emissions, H_β, λ4278Å of N_2^+, λ5577Å of [01], and λ6300Å of [01] were plotted against local mean geomagnetic L time (defined in chapter II) for each night of observations. The λ4278Å, λ5577Å and λ6300Å emissions show a tendency to vary together, though there is no constant relationship between them. These emissions are all excited mainly by electrons and the tendency to vary together is expected. The intensities and their inter-relationships depend upon the energy spectrum and flux of the electron precipitation. H_β shows little relationship with the electron excited emissions.

Average curves for the four emissions for the months July to September 1966 are shown in Figure 8. λ4278Å, λ5577Å and λ6300Å show peak emission just prior to local L midnight. The H_β curve has a peak at $16^h\ 30^m$.

Night-time cosmic radio noise absorption events at Mawson can usually be classified, following EATHER and JACKA (1966a), as Sudden Ionospheric Absorption (SIA), with duration of order 10 minutes, or Slowly Varying Ionospheric Absorption (SVIA), with duration 3/4 to 1½ hours. SIA are typically associated with discrete auroral forms especially in the evening hours. SVIA are generally initiated by an SIA of 1 to 2 db (occasionally up to 10 db) while in the main phase absorbtion amplitude is usually 0.3 to 1.0 db.

During SIA a large increase in λ5577Å intensity is usually recorded together with moderate increases in the other emissions, except

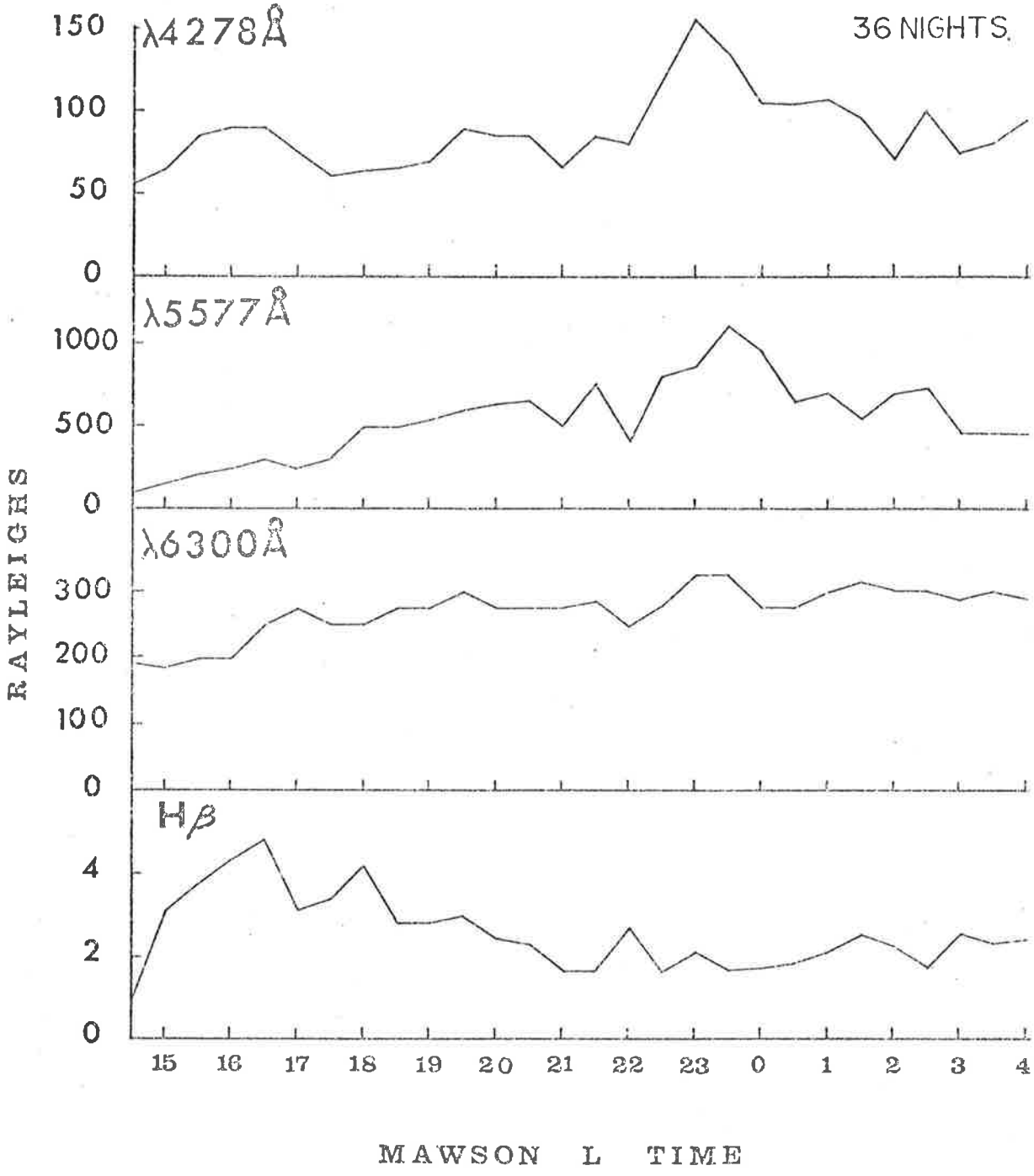

Fig. 8. Average curves of the variation in intensity of the four emissions plotted against L time.

H_β shows no correlation with SIA events. During SVIA moderate increases in all emissions including H_β occur. Generally, during the first 10 minutes of an SVIA, discrete auroral forms typical of the breakup phase of the auroral display are in the zenith, implying that during this phase the absorption is really SIA in type, i.e. directly related to the λ5577Å emission. Following this the all sky pictures show diffuse emission, and the occasional segment of an arc (usually faint); this phase is the SVIA part of the absorption.

During an SVIA negative bays always occur in the H-trace magnetogram. The times of onset of the SVIA and the negative bay agree well, with the time of the maximum of the bay usually agreeing with the time of the maximum absorption. The end times do not always agree, though this may be due mostly to the difficulty in specifying the end of either the bay or the SVIA.

H_β emission occurred during every SVIA event recorded. EATHER and JACKA (1966a) and FRANCIS and JACKA (1969) also observed this at Mawson. Plotting the half hour averages of the four emissions with the SVIA onset time as origin yields Figure 9. Considerable order is now presented to the data. Each emission follows the same pattern, with the intensity rising to a maximum at the SVIA onset, falling to a minimum just prior to the onset and displaying a broad period of enhancement 4 to 6 hours before the SVIA onset. Individual records show the same features after the SVIA but in the preceding hours are typically highly irregular.

By studying the SVIA events at Stations a few hours east of Mawson, it was thought some order may be apparent in the pre-SVIA onset hours.

As there are no Antarctic stations a few hours east of Mawson,

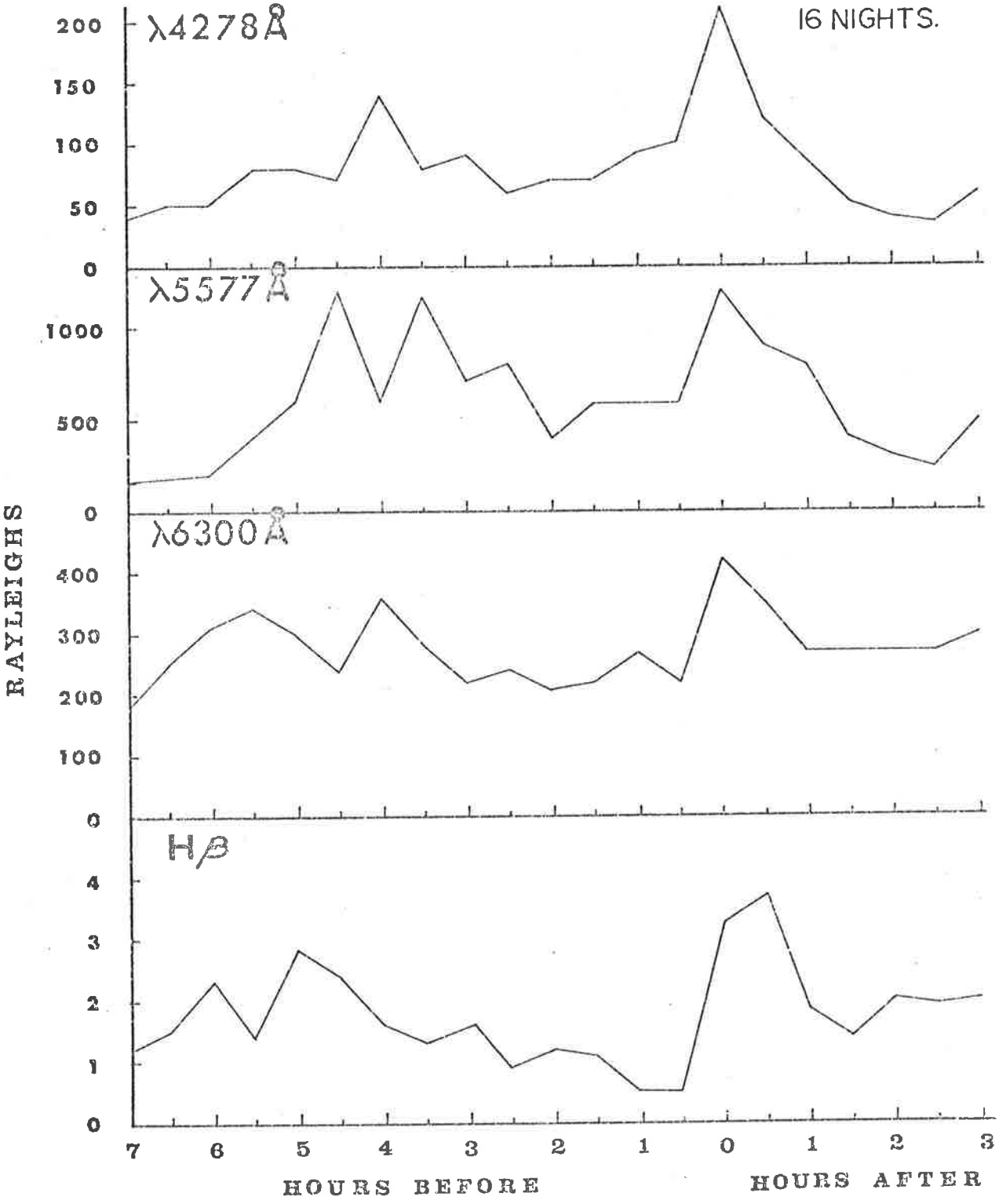

Fig. 9. Average curves of the variation in intensity of the four emissions plotted with SVIA event onset time as zero.

Northern Hemisphere stations a few hours east of Mawson conjugate were sought. Kiruna and Murmansk were used. The L co-ordinates of the stations are

Mawson	28°E	71°S
Mawson conjugate	28°E	71°N
Kiruna	36°E	65°N
Murmansk	48°E	66°N

It was thought that since Kiruna was about 8° east of Mawson, SVIA events would occur about half an hour before those at Mawson, and those at Murmansk $1\frac{1}{3}$ hours before those at Mawson.

During the period February to September 1966, Mawson had 26 SVIA events, and Kiruna 27. Of these 18 started at the same Universal Time at both stations.

Only records from July to September 1966 were to hand for Murmansk. During this period Murmansk had 9 SVIA events, Mawson 18, and Kiruna 12. Kiruna and Murmansk had 6 events with simultaneous onset times, during this period, whilst Mawson, Kiruna and Murmansk had three simultaneous onset SVIA events.

MANTLE AURORA:

SANDFORD (1964, 1968) found that the contours of constant mean intensity of the mantle aurora, defined as the widespread glow that covers most of the sky in auroral regions, formed along lines of constant colatitude and not parallel to the auroral oval. His criterion for the measurement of the mantle aurora was that there be no discrete visual aurora in the sky at the time.

The present work confirms Sandford's results, but suggests that the criterion of no discrete visual aurora in the sky, whilst useful, is rather crude as subvisual discrete aurora may confuse the overall picture.

PROTON AURORA INTENSITY RATIOS:

EATHER (1968) measured the ratio of the intensities of λ3914Å N_2^+, λ4709Å N_2^+, λ5577Å [01] and λ6300Å [01] emissions to the intensity of the H_β emission, from the premidnight proton excited arc as it moved toward lower latitudes at Fort Churchill (L Latitude 72°N) and found agreement with theoretical ratios he derived.

Ratios similarly measured at Mawson for λλ5777Å and 6300Å are typically much greater and show a much greater scatter than did Eather's.

(b) DISCUSSION

The average diurnal intensity variations of λ5577Å and λ6300Å are not inconsistent with those of SANDFORD (1968), which were based on patrol spectrograph data from seven southern hemisphere stations during 1963. Sandford did not report on λ4278Å or H_β. He found no peak in the average λ5577Å emission at about local L midnight as was found at Mawson. The patrol spectrograph method is crude and the results are given in terms of iso-rayleighs plotted on a latitude/ corrected geomagnetic time (HAKURA 1965) grid, in sequential steps of 0, 0.25, 0.5, 1.0 etc. kilorayleighs. Using such a procedure the small midnight peak observed at Mawson would be unlikely to show up in Sandford's work.

The diurnal H_β curve peaks at $16^h\ 30^m$ L at Mawson. The low midnight average is at first sight surprising. The SVIA- onset- as- zero H_β curve displays a broard rise several hours before the onset. If each night is taken seperately and plotted against L time the broad rises tend to overlap resulting in the maximum at $16^h\ 30^m$ L, whereas the narrow rises during the SVIA tend not to overlap resulting in an overall low average value.

EATHER and JACKA (1966b) point out that the H_β Fraunhofer absorbtion in the continuous spectrum of scattered sunlight at dawn or dusk, or of moonlight could result in the apparent reduction of the true auroral H_β signal. The H_β diurnal curve of Figure 8 is for moonless nights, and for times not effected by twilight contamination.

The Milky Way contribution of H_β can be up to 65 Rayleighs at λ4861Å at Mawson (EATHER and JACKA 1966b). It is easily distinguishable in the rocking filter technique (see EATHER and JACKA 1966b) due to the fact

that it is not doppler shifted and is of much narrower profile than the auroral H_β. The two filter technique does not allow this unshifted galactic contribution to be recognised. Milky Way H_β is known to useful accuracy (MONTBRIAND et al., 1955, RODGERS et al., 1960), but only to about -15° New Galactic Latitude.

The period of these H_β measurements corresponds largely with the time when the Mawson zenith points to a region of the galaxy of New Galactic Latitude lower than -15°. FRANCIS (1967) used an image intensifier to monitor H_β at Mawson during July, August and September 1964. He shows an image intensifier picture of strong H_β emission from the Milky Way during this period, indicating that the possibility of Milky Way contamination cannot be disregarded.

AKASOFU (1964) on the basis of I.G.Y. all sky camera records from an almost continuous chain of stations with overlapping fields of view, in the northern auroral region, formulated the concept of the global auroral substorm to describe the dynamic morphology of visual aurora. Recently, AKASOFU (1968) has extended this concept to include other aurorally associated phenomena.

Figure 10 depicts the growth and decay of Akasofu's model of the auroral substorm (A→B→C→D→E→F→A). The auroral substorm has two characteristic phases; the expansive phase and the recovery phase. The first indication of the substorm is a sudden brightening of one of the quiet arcs lying in the midnight sector of the oval or a sudden formation of an arc (B,T=0-5 min). In most cases, the brightening of an arc or the formation of an arc is followed by its rapid poleward motion, resulting in an 'auroral bulge' around the midnight sector (C, T=5-10 min). The so-called 'break-up' phenomenon occurs

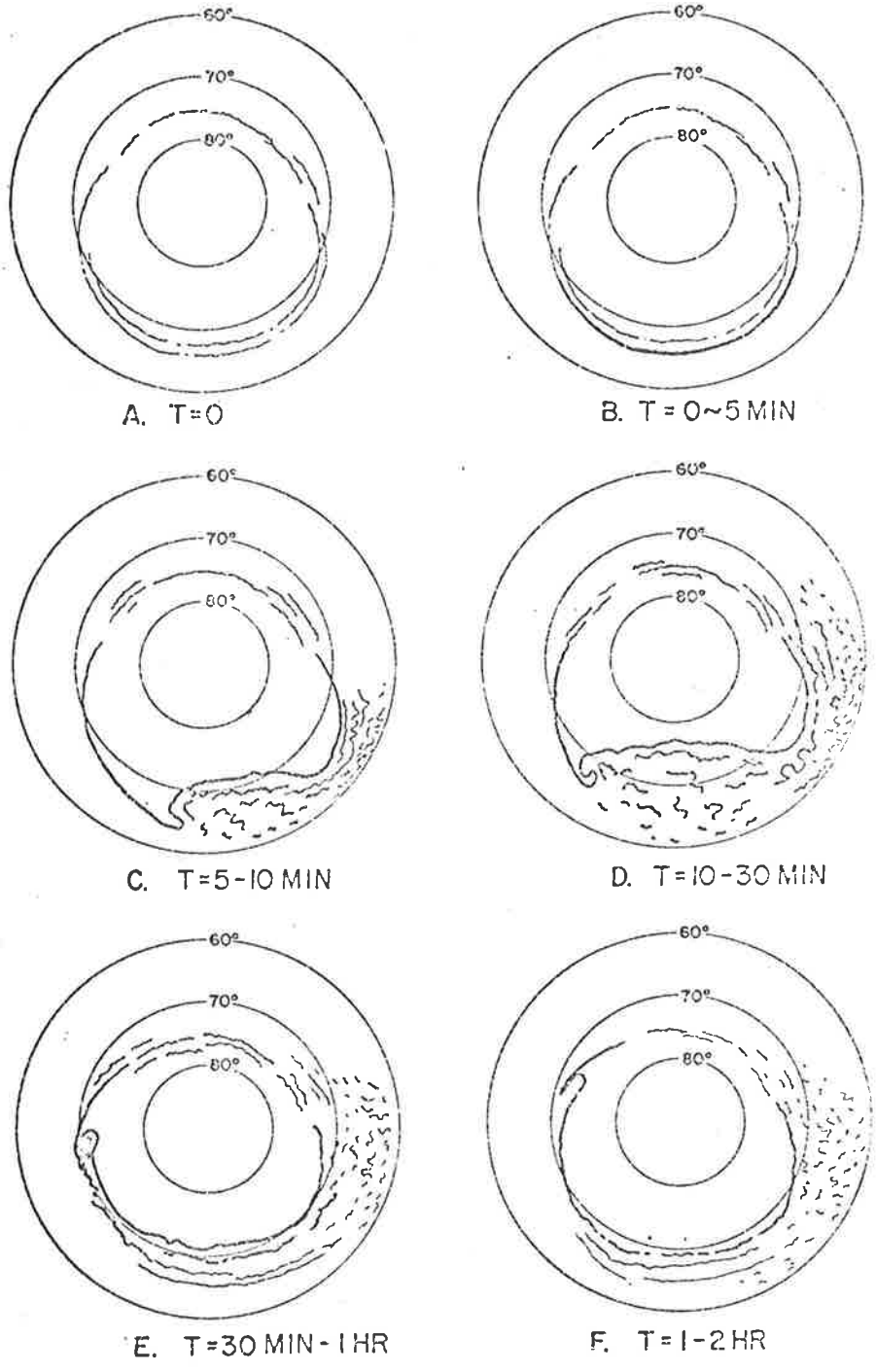

Fig. 10. Schematic outline of the development of the auroral substorm (AKASOFU 1968).

in the bulge, but it is not the whole display. As the auroral substorm progresses, the bulge expands in all directions (D, T=10-30 min.). In the evening side of the expanding bulge, a large-scale fold appears which travels rapidly westward along an arc, namely, the westward travelling surge. In the morning side of the bulge, arcs appear to disintegrate into 'patches' which drift eastward with a speed or order 300 m/sec.

When the expanding bulge attains its highest latitude, the recovery phase of the auroral substorm begins (E, T=30 min-1 hour). The expanded bulge begins to contract. The westward travelling surge may still travel a considerable distance after the end of the expansive phase, but it degenerates eventually into irregular bands. In the morning sky, eastward drifting patches remain until the very end of the recovery phase (F, T=1-2 hours). At the end of the substorm, the general situation will be similar to that just before the onset of the substorm.

AKASOFU's (1968) exposition of the proton aurora substorm is outlined in Figure 11, where the hatching indicates the proton emission regions superimposed upon the visual aurora substorm scheme, at four states of the substorm, T=0, 5-10 min, 10-30 min and 30 min - 1 hour. During the quiet periods between substorms, the proton precipitation occurs along an oval band which is located a little equatorward of the auroral oval. In the midnight meridian the precipitation occurs over the centre region of the auroral bulge, so that the precipitation area expands rapidly poleward. In the evening sector the proton aurora shifts rapidly equatorward during an early phase of the substorm. However, westward travelling surges which had advanced well into the evening sector do not appear to contain the hydrogen emissions. In the morning sector, the hydrogen emission seems to

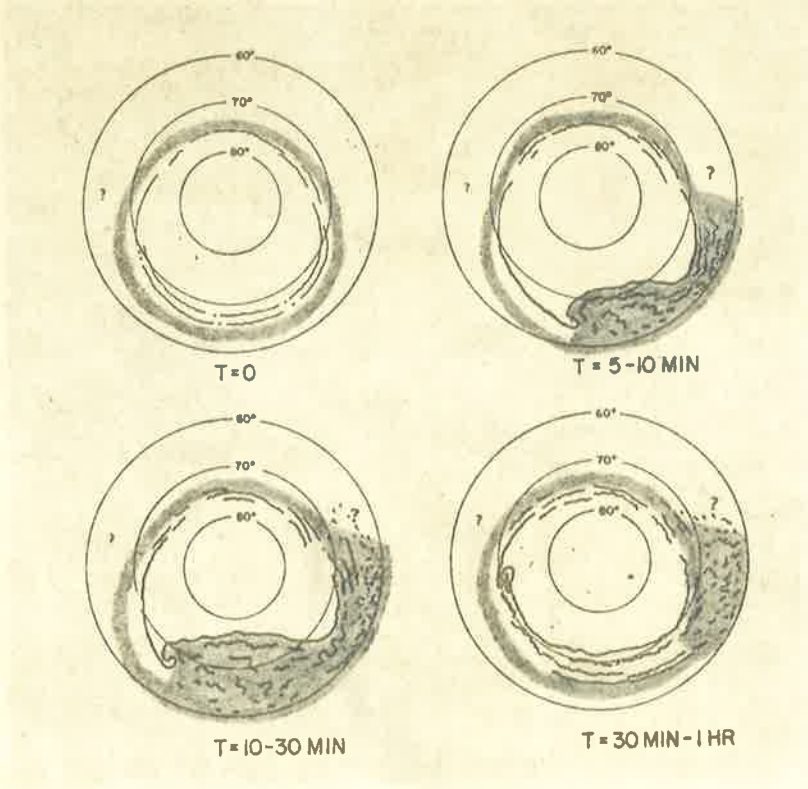

Fig. 11. Development of the proton aurora substorm (AKASOFU 1968).

appear over an extensive area. The extent of the morning precipitation area is not known, Akasofu adds.

Figure 12 are histograms of the frequency of occurrence of the onset times of SVIA events for Kiruna and Mawson. All but two of the SVIA occurred within three hours of local L midnight with the peak occurrence at L midnight.

The poleward auroral bulge in Figure 10D covers a longitudinal extent of about 90°, corresponding to about 6 hours, indicating that any auroral phenomenon tied to the bulge would occur within + or - three hours of local L midnight. As Mawson and Kiruna SVIA onset times have a similar range, this strongly suggests that SVIA events are features of the poleward auroral bulge.

All the features of SVIA events can be correlated with aspects of the auroral substorm. The small SIA that initiate the SVIA correspond to the bulge front passing overhead. This front is highly active and consists of fragments of arcs and patches which move or shimmer quickly, resulting in relatively small overall absorption.

The SVIA corresponds to the diffuse luminosity and occasional faint patch that fill the bulge. ANSARI (1964), EATHER and JACKA (1966b), and BAILEY (1968) all conclude that SVIA are associated with a hardened electron precipitation. H_{β} emission appears to occur during both the initial SIA and the main phase of the SVIA within the bulge.

The magnetometer measures the net effect of all electric currents both near and far, but gives most weight to near disturbances, manifesting these effects in a negative bay. The fact that the negative bay starts at about the same time (within ± 2 minutes, the time resolution of the record-

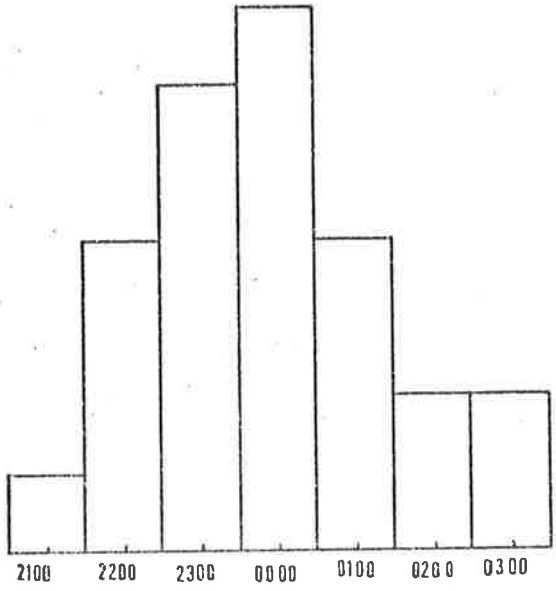

MAWSON
(26 events)

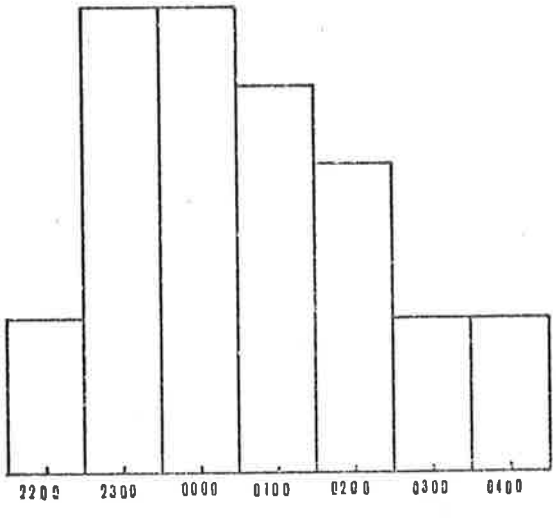

KIRUNA
(27 events)

Fig. 12. Frequency of occurrence of SVIA events with local L time for Kiruna and Mawson.

ing charts) as the ionospheric absorption indicates that the bulge front must move quite quickly over Mawson, otherwise the bay would precede the absorption.

Finally the duration of SVIA events from 3/4 to about 2 hours is consistent with the position of Mawson (L latitude about 71°) with respect to the various phases and the duration of the substorm in the midnight sector.

Figure 9 indicates that there are differences in the times of the peaks of emission in the several wavelengths in the period 4 to 6 hours before the SVIA onset time. These peaks correspond to the passing of Mawson under the quiet auroral arc region. Consideration of Figure 11 indicates that the peak in H_β emission should occur about one hour before the peak in λ5577Å emission at Mawson, and that the λ5577Å emission peak should occur about 5 hours before the SVIA onset.

The peak emission in λ5577Å and λ4278Å (Figure 9) occurs about 4 hours before the SVIA onset and the peak emission in H_β occurs about 5 to 5½ hours before the SVIA onset. Thus the broad features of Figure 9 are in agreement with the auroral substorm model.

However, the peak in λ6300Å emission occurs at about the same time as does the H_β peak, suggesting that the electrons responsible for λ6300Å emission may form a distinct zone that corresponds closely to the proton emission zone or that a significant part of the λ6300Å emission is excited by protons. These conclusions are tentative however as there is insufficient data to make conclusive inferences.

The apparent simultaneity of SVIA onsets at Mawson, Kiruna and Murmansk is consistent with the auroral substorm model. One might expect some difference in onset times at these stations as the bulge front must

have a finite velocity. The time resolution of the riometer records from Kiruna and Murmansk is however about 10 minutes; thus differences in onset times as small as 15 minutes could not be ascertained.

The appearance of SVIA at one station and not at the others is also explainable. It should be remembered that Figures 10 and 11 are representative of a mean situation. Each substorm differs in total amount of activity, the size of the instantaneous quiet auroral oval and the position of the bulge on the earth. It is conceivable that SVIA could occur at one station and not at the others because they are poleward of the bulge region. Hence any permutation of occurrence and non occurrence at the three stations is consistent, except that one would expect that simultaneous occurrences at Mawson and Murmansk would be accompanied by an event at Kiruna also, (unless the emission in the bulge is very patchy). On the three occasions when SVIA were simultaneous at Mawson and Murmansk an SVIA occurred simultaneously at Kiruna.

The results of EATHER and JACKA (1966b) indicate that the relationship between H_β and the auroral breakup, and hence, presumably, the polewards bulge is not so straight forward. They found that during the hour or so before the auroral breakup the H_β intensity gradually decreased to a low level, often zero, in the zenith and to the south. There was still appreciable emission in the north. This suggests that the fall in intensity is due to the zone moving north of the station rather than an overall decrease in the brightness of the emitting region. During and after the breakup event, the H_β intensity increased over the whole sky to about the same level as earlier in the night. The proton emission at this stage seemed to be associated with the diffuse patchy luminescence that usually covered the

sky after breakup. Scans across the sky during such periods showed, however, that although the visual radiation was patchy spatially, the hydrogen emission was uniformly distributed. They also found that auroral breakup events accompanied by post breakup glow often occurred without detectably enhanced H_β.

Of the past work on cosmic radio noise absorption little has been done on the midnight SVIA (Akasofu's "M" type absorption). Much work has been carried out on the daytime M events (FEDYAKINA 1963, BROWN 1964, ANSARI 1965, JELLY and BRICE 1967, BEWERSDORFF et al. 1967, BEWERSDORFF et al. 1968). The daytime M events are not considered here.

Several studies have been made that do not distinguish between the various types of absorption (HARTZ et al. 1963, HARGREAVES and COWLEY 1967, HOOK 1968) and hence, if, as seems to be the case (ANSARI 1965, EATHER and JACKA (1966b), BAILEY 1968) different energy spectra of the precipitated electrons are associated with different types of absorption events, these studies are of limited use.

ANSARI (1965) investigated night time SVIA and invoked a hardened electron energy spectrum to explain them. EATHER and JACKA (1966b) reached the same conclusion. BAILEY (1968) in a review of the subject, puts forward a simple theory that supports this hardened spectrum view.

The observations of EATHER and JACKA (1966a, 1966b), FRANCIS and JACKA (1969), and the present observations were made at Mawson (L latitude 71°), and all observations of SVIA were made within about 3 hours of local L midnight. However, BERKEY (1968) reports on two SVIA from College (L latitude 66°) at $4^h\ 30^m$ and 5^h local time on the 25th and

26th January 1966, during which no H_β emission occurred.

Berkey's 26th January event (the 25th January is not shown) is very smooth, not initiated by the usual SIA, and looks like a day time event. The photometer records indicate that a pulsating auroral patch was above the station.

However the time of these events is such that the 100 km region was well inside the earth's shadow, hence they cannot be construed to be day time events. Predawn conjugate effects are also precluded. This absence of H_β is puzzling.

The reason for the absence of H_β could be one of many:

i) H_β emission only occurs during SVIA events associated with the poleward bulge in the midnight sector (usually within ±3 hours of local L midnight.) Berkey's events occurred at $4^h\ 30^m$ and 5^h local L time and the photometers indicate that there is no breakup event prior to these SVIAs indicating that these "predawn" events may be of a different class to the bulge type.

ii) The H_β emission is dependant strongly on L latitude, and that College (66°N) is too low to register H_β whereas Mawson (71°S) is better situated.

iii) SVIA and H_β emission are not causally linked even in the poleward bulge region.

iv) EATHER and SANDFORD (1966) found that H_β emission varies greatly during the solar cycle, and in January 1966, very low H_β values would be expected. It may be that Berkey's H_β photometer was not sensitive enough to detect these low values of H_β (The Mawson results indicate that levels of about four Rayleighs would be expected).

It is interesting to note that the records reproduced in Berkey's paper show an SVIA commencing at about $1^h\ 15^m$ local L time on the 26th January, some 4 hours before the no-H_β-SVIA event. During the $1^h\ 15^m$ event H_β enhancement is just discernible from his published records throwing suspicion on his H_β photometer sensitivity.

MANTLE AURORA:

Following SANDFORD (1964, 1968) the average intensities of emission at λ4278Å N_2^+, λ5577Å [01] and λ6300Å [01] when the all sky camera indicated that no discrete aurora was present, were plotted against L time for the two Kp intervals 0^- to 1^+ and 2^- and higher (see Figure 13).

If the mantle aurora had the global distribution of the quiet auroral oval, we would expect two peaks in each plot for each emission, at about $21^h\ 30^m$ and $2^h\ 30^m$ L time for Mawson. These times are when the auroral oval is intersected by the passage of Mawson (L Latitude 71°S) under it (see Figure 10A).

The gap in the plot (Figure 13) for each emission for Kp $>2^-$ indicates that discrete auroral forms occurred on each night of observations between 23^h and 2^h L time.

The λ4278Å N_2^+ plots show no significant diurnal variation. The λ5577Å [01] plots show peaks at about $21^h\ 30^m$ and $1^h\ 30^m$ for Kp between 0^- and 1^+ and a single peak at 19^h for Kp $>2^-$. The λ6300Å [01] plots show a large single peak at about 2^h for the lower Kp range and a single peak at about $3^h\ 30^m$ for the higher Kp range.

No overall consistency in the patterns of the diurnal variations is shown between the six plots. Certainly there is no tendency towards

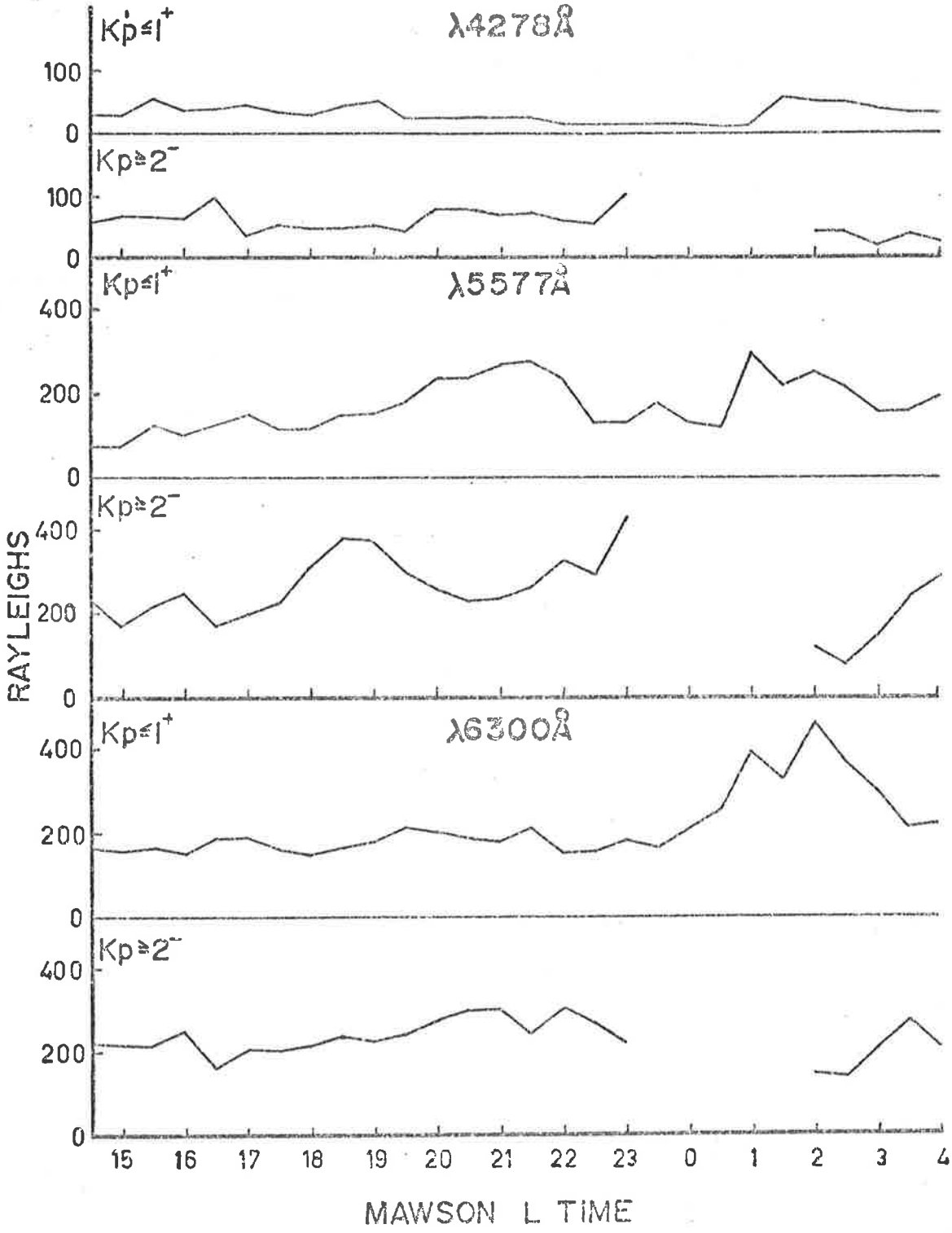

Fig. 13. Plots of mantle aurora intensity against L time for Kp < 1^+ and Kp > 2^- for λ4278Å N_2^+, λ5577Å O1 and λ6300Å O1 emissions.

peaks at $21^h\ 30^m$ and $2^h\ 30^m$ as a quiet auroral oval distribution requires. However these results are not inconsistent with those of Sandford.

The diurnal variation of λ5577Å and λ6300Å for those periods of each night when no discrete auroras were visible, is such, especially for Kp $>2^-$, that it is unlikely that the variation was due only to the mantle aurora and the background airglow, but rather to subvisual discrete auroras also. Indeed the records of each individual night show rapid fluctuations characteristic of discrete visual aurora.

PROTON AURORA INTENSITY RATIOS:

EATHER (1968) measured the ratio of the intensities of λ3914Å N_2^+, λ4709Å N_2^+, λ5577Å [01] and λ6300Å [01] emissions to the intensity of H_β in the pre-midnight proton excited arc as it moved towards lower latitudes at Fort Churchill (L latitude 72°N). His results show a consistent trend and he quotes his + and -1 standard deviation values of the mean ratio for λ5577Å to be 12.5 and 9.0 and for λ6300Å 3.3 and 2.5.

Figure 14 shows the Mawson plots for these two wavelengths. The scatter in the Mawson results is much greater than in Eather's and the ratios much greater. Even taking the minimum plausible ratio represented by the lines on Figure 14 the ratios are 20 for λ5577Å and 16 for λ6300Å.

The disparity between the two sets of results is difficult to explain, except by suggesting that at Mawson the proton precipitation is always accompanied by electron precipitation. It should be noted that Eather's H_β values (up to 300 Rayleighs) are relatively high, whereas the Mawson values (below 20 Rayleighs) are relatively low. Further work is needed to clarify this point.

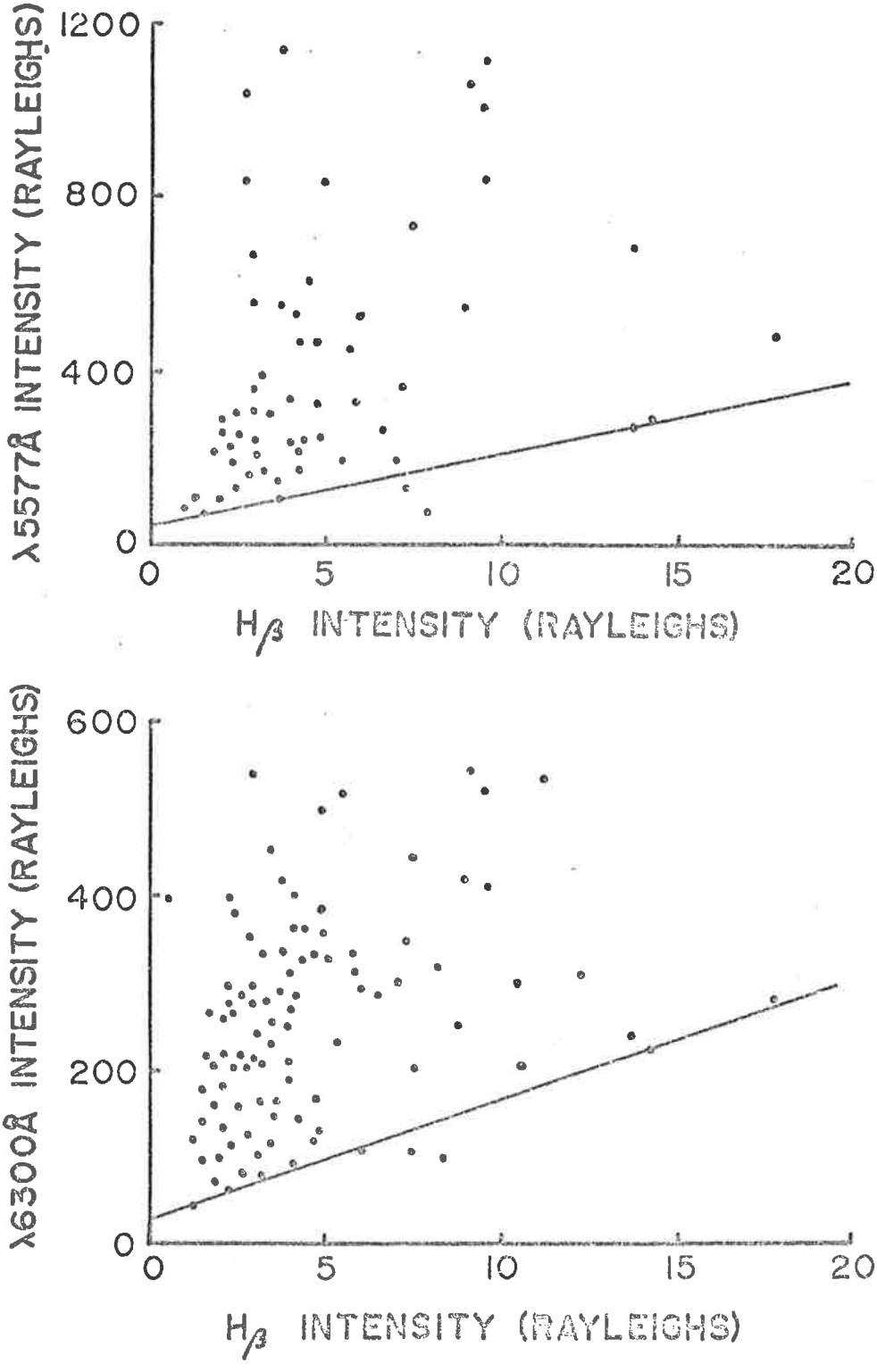

Fig. 14. The intensity of λ5577Å [01] and λ6300Å [01] plotted as a function of the associated H_β intensity in the pre-midnight proton excited arc.

CHAPTER V THE LUMINOUS PATCHES

On the morning and on the evening of August 11th and on the evening of August 14th, 1966, patches of faint blue-white luminosity were seen in the twilight sky, at Mawson. The colour and solar depression angle suggested that these patches may be rare noctilucent clouds.

Noctilucent clouds (NLC) occur usually at a height of about 82 km. This is the height of the mesopause, where the lowest temperature in the earth's atmosphere occurs. The nature and origin of these clouds is not well understood.

These clouds are seen against the background of a dark sky while they are still illuminated by sunlight, when the sun is well below the horizon. They generally resemble cirrus or cirrostratus cloud, often having a delicate filigree pattern, with a marked wave structure. They are generally tenuous so that stars shine through them undimmed. They are most often observed in the summer months at high latitudes.

NLC are to be distinguished from nacreous, or mother of pearl clouds which are formed at an altitude of 17 to 35 km at high latitudes during the winter months.

In order that the NLC may be visible from the ground: (1) the sky must be relatively free of tropospheric clouds, (2) the mesopause must be sunlit - this condition is fulfilled when the sun is not more than 16° below the observer's horizon, and (3) the sky background must be dark enough for the clouds to stand out - this requires that the sun is at least 6° below the horizon.

The geometry of NLC sighting is shown in Figure 15. An observer at O can see NLC at the 82 km level over an arc extending in the vertical through the sun between angular elevations κ, κ' when the true solar depression angle is α. At elevation angles less than κ, the sky background is too bright for the NLC to be visible, and at elevation angles greater than κ', the NLC are no longer illuminated. The angles, κ, κ' are functions of the solar depression angle, the NLC height, and the screening height (H_{SC}) of the earth's atmosphere.

Sunlight passing closer to the earth than a height H_{SC} is so greatly attenuated by scattering and absorption that only those rays passing above this height have sufficient intensity to make NLC visible.

The NLC observation period (solar depression angle = 6° to 16°) varies markedly with latitude and season. A relationship between the true solar depression angle α, the solar declination δ, the hour angle τ, and the latitude of the observer λ, is

$$\sin \alpha = -\sin\delta\sin\lambda - \cos\delta\cos\lambda\cos\tau \qquad \ldots(1)$$

From this equation, the local mean time at which a given solar depression angle occurs on a particular date for a particular latitude may be determined. Using this proceedure Figure 16 showing the observation periods throughout the year for Mawson (67.6°S) was constructed.

A useful method of estimating the approximate height of NLC is based on considerations of the height (H_{SH}) of the shadow of the solid earth plus atmospheric screening layer at the time the upper border of the NLC fades from view. Figure 17 shows the dependence of the shadow height in the sun-cloud-observer plane on elevation angle for a screening height

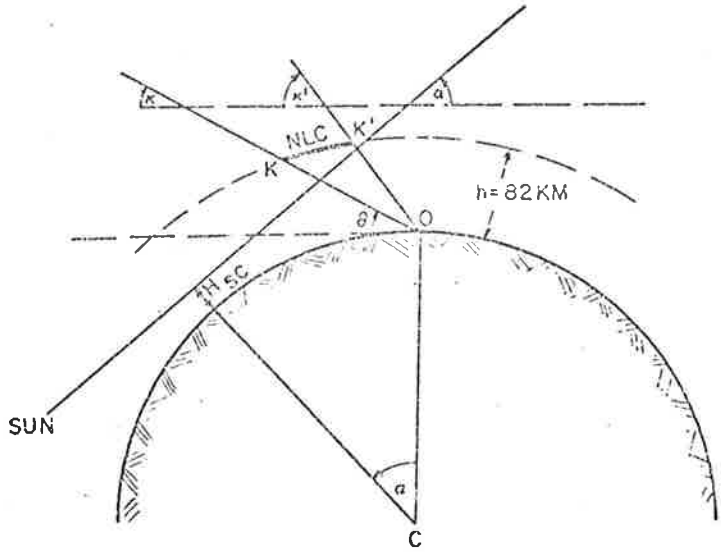

Fig. 15. Illustration of the conditions under which noctilucent clouds may be seen, (after FOGLE 1966). For explanation see text.

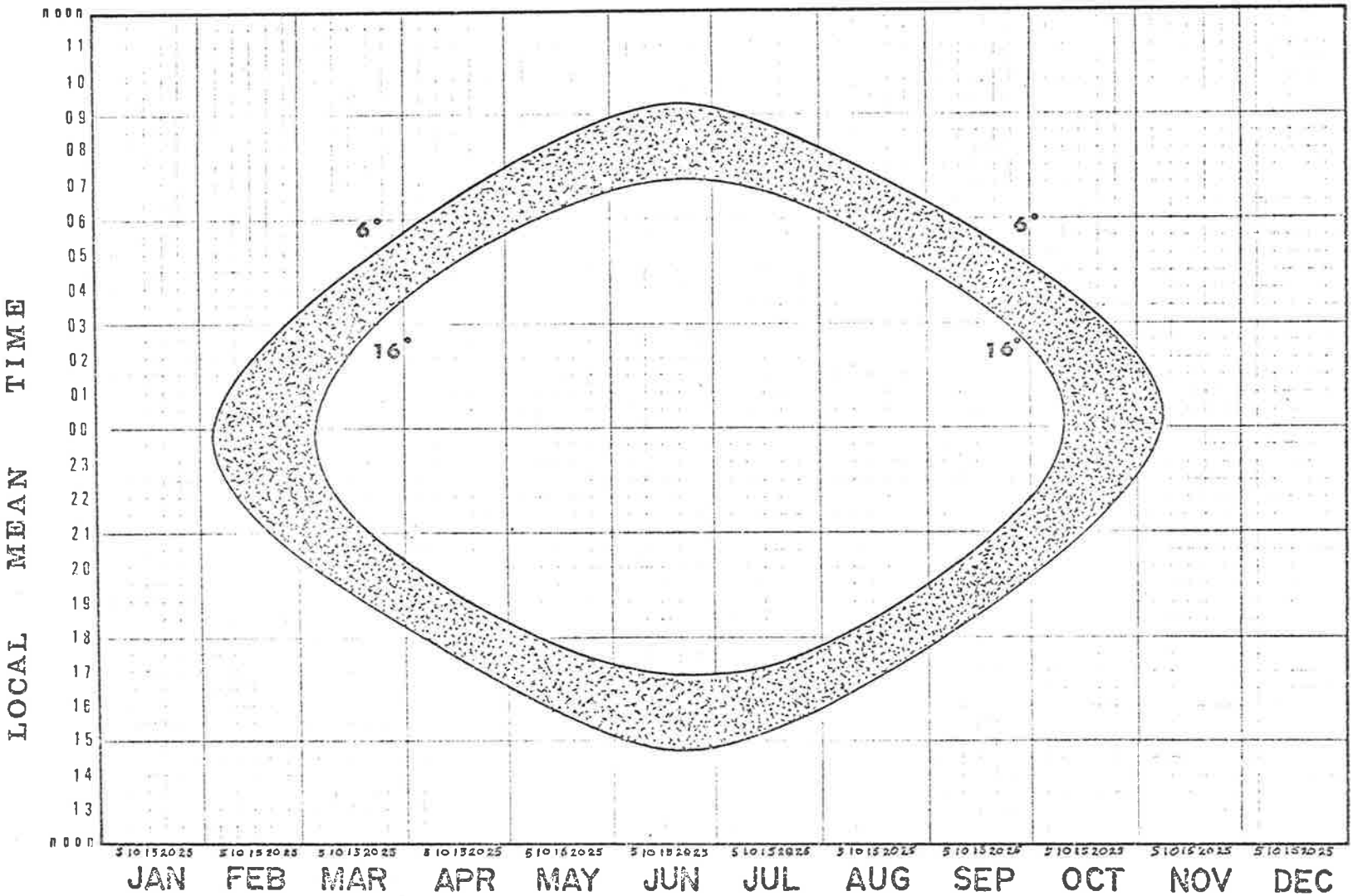

Fig. 16. Noctilucent clouds are usually observed in the hatched time interval, which corresponds to a true solar depression angle between 6° and 16°, at the latitude of Mawson (67.6°S).

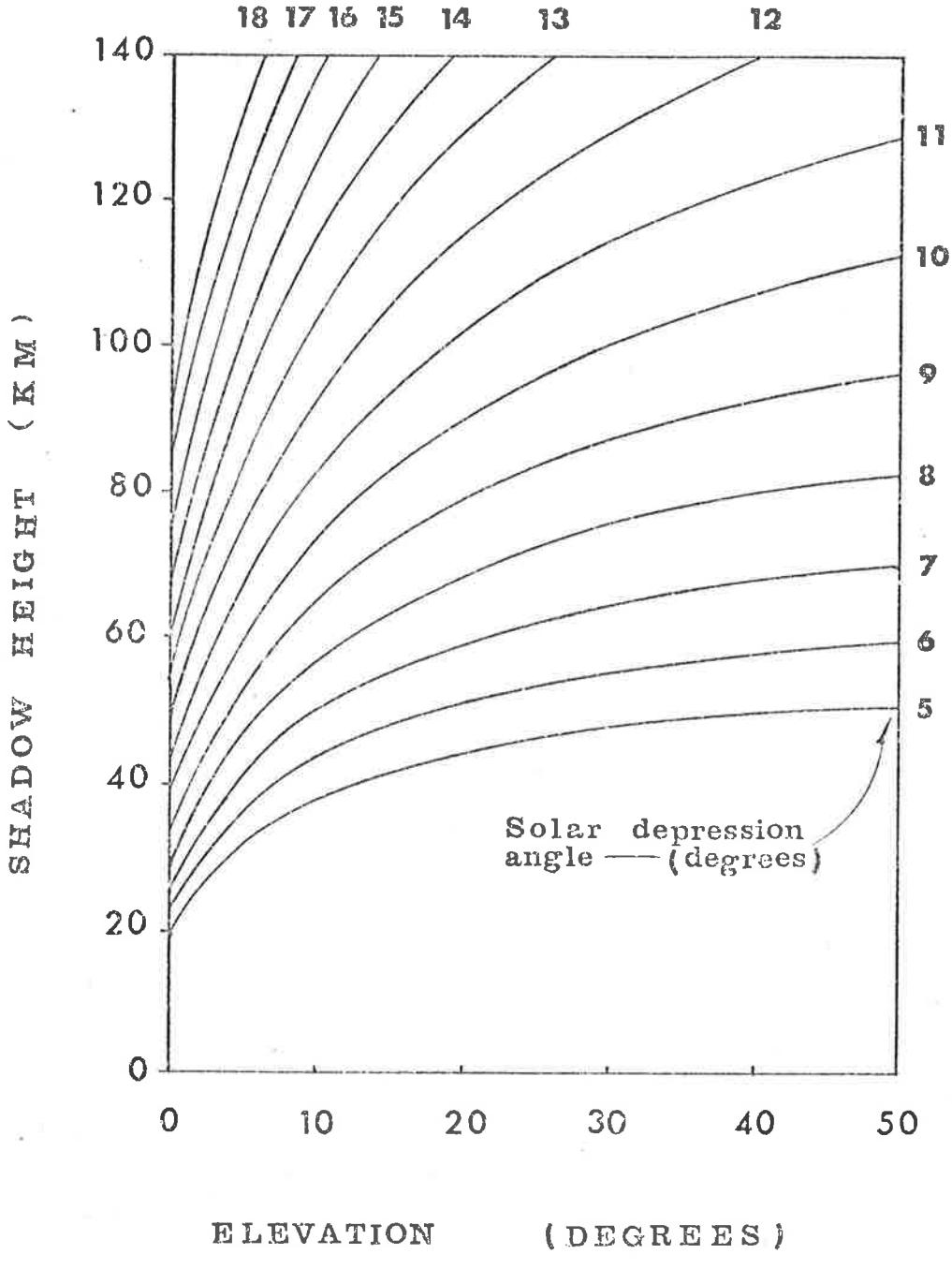

Fig. 17. Nomogram relating the earth shadow height to elevation angle and true solar depression angle for a screening height of 30 Km, (after FOGLE and HAURWITZ 1966).

of 30 km, a figure derived from both theoretical considerations (CHAMBERLAIN 1961 and FOGLE and HAURWITZ 1966) and measurements (see FOGLE and HAURWITZ 1966).

The August 11 and 14 sightings fitted the conditions for NLC viz. (1) $6^{\circ} < SDA < 16^{\circ}$ (2) the sky was free of tropospheric clouds and (3) they were bluish-white in colour. They were reported (KILFOYLE 1968 - see Appendix) as such.

These sightings occurred during the Perseids meteor shower. Other sightings (HAMILTON 1964, FOGLE 1966) of NLC have occurred during meteor showers. However, FOGLE and HAURWITZ (1966) had examined the northern hemisphere data and concluded that no relationship exists between the showers and NLC. Table 1 lists all the known reliable southern hemisphere sightings of noctilucent clouds, together with relevant meteor showers and their maximum rate dates, extreme limit dates and declinations.

Six out of the eight displays (treating as one display any series of displays on near nights) occurred during a meteor shower. The display of January 9 may have occurred close enough after the Quadrantids (January 1-4) to be related to it. The display of January 17, 18 and 20, however, cannot be related to any meteor activity.

The excellent agreement found on December 4-5, October 30, and February 8 and 12, August 11 and 14 and in particular January 1-4, seems to imply some relationship between these two phenomena; however, even among these showers the declinations are such that only the Phoenicids and the Taurids can be seen at the latitudes of the sightings. This, together with the display of January 17, 18 and 20, makes it difficult

TABLE 1 SOUTHERN HEMISPHERE NOCTILUCENT CLOUD SIGHTINGS

DATE	PLACE	METEOR SHOWER	MAXIMUM	EXTREME LIMITS	DECLINATION	REFERENCE
4/5 Dec. 62	Ship 55°S, 58.8°W	Phoenicids	Dec. 5	Dec. 5	-55	See FOGLE (1966)
30 Oct. 64	Mawson 67.6°S, 62.9°E	N. Tuarids S. Taurids	Nov. 12 Nov. 1	Oct.17-Dec.2 Oct.27-Nov.22	+21 +14	FRANCIS et al (1966)
9 Jan. 65	Punta Arenas 53.1°S 71°W	-	-	-	-	FOGLE (1965)
8 Feb. 65) 12 Feb. 65)	Mawson	Aurigids	Feb. 9	5 days ?	+38	FRANCIS et al (1966)
25 Dec. 65) 29 Dec. 65)	Punta Arenas	Ursids	Dec. 22	Dec.22-23	+80	FOGLE (1966)
1 Jan. 66 2 Jan. 66 3 Jan. 66 4 Jan. 66	Punta Arenas	Quadrantids	Jan. 3	Jan. 1-4	+50	FOGLE (1966)
17 Jan. 66 18 Jan. 66 20 Jan. 66	Punta Arenas	-	-	-	-	FOGLE (1966)
11 Aug. 66 (AM)) 11 Aug. 66 (PM)) 14 Aug. 66)	Mawson	Perseids	Aug. 12	July29-Aug.17	+58	Herein

to see how there could be any relationship.

FOGLE (private communication) indicated that the observation of NLC during winter was unexpected. Theoretical considerations show that the mesopause temperature must be less than about 145°K for NLC to form. The NASA rocket soundings at Fort Churchill indicated temperatures of around 140°K during the summer months and around 200°K during the winter months. If these results are applicable to the southern hemisphere one would not expect NLC to occur there during the winter months. Also, he pointed out, the past NLC data from both hemispheres suggest that these clouds do not occur in winter. The many reports of winter NLC had always turned out to be either aurora, nacreous clouds (essentially a winter time phenomenon) or sunlit or moonlit cirrus, he added.

The morning display of August 14 was not seen by the author and no measurements were taken of it. However from the description, time and position, it had all the characteristics of NLC. The relevant information relating to the two evening displays is:

	Time (U.T.)	S.D.A.	Bearing	Elevation
August 11	1300 to 1415	9.3° to 16.3°	236 to 297°E	10 to 12°
August 14	1320 to 1420	10.3° to 16.0°	248 to 281°E	10 to 12°

Also, Mawson: 67.6°S, 62.9°E

Mawson LMT = U.T. + 4^h12^m

The moon position on August 11 and 14 was such that the patches could not be moonlit. For a SDA of 9° (the SDA corresponding to the earliest observation time of the patch) and a screening height of 30 km,

the earth's shadow height (from Figure 17) is about 65 km. Clearly nacreous clouds at 25 km cannot be sunlit at that time. As cirrus cloud occurs at heights lower than nacreous, this possibility is eliminated also.

A copy of the colour slide (Plate 2) taken of the August 14 display was sent to Fogle. The data relevant to the photograph are:

Film:	Kodachrome II
ASA rating:	25
Exposure:	2 mins.
Aperture:	f/1.8

FOGLE (private communication) after examining the photograph concluded that it was an aurora; either part of a homogeneous arc or a cloud-like aurora similar to Figures 2 and 7 in STORMER (1955). He claims that the diffuse structureless patch shown on the colour slide lacks the characteristic structure and form of a NLC and the colour is too blue and too uniform for NLC. He mentions that on several occasions in Alaska he has seen diffuse aurora (sometimes sunlit) with the blue colouration, and the structureless, diffuse form shown, on the slide.

Sunlit aurora usually have a green (due to $\lambda 5577\text{Å}$ [01]) and or violet (due to $\lambda\lambda$ 3914Å and 4278Å of N_2^+) colour, whereas NLC usually have a bluish-white colour.

From the recommended exposure given by FOGLE (1964) of one minute at f/3.5 on 25 ASA film, Plate 2 would be overexposed by a factor of about 8. If this is so then any fine structure would be lost. FOGLE (1964, 1966) shows colour prints of NLC in which the structure would surely disappear if overexposed by this factor.

From inspection of Plate 2 it is apparent that the patch was not

Plate 2. The August 14 patch of luminosity.

part of an auroral arc as defined in the International Auroral Atlas (1963). All sky camera records (one frame per minute) indicate the patch remained stationary for 1¼ hours on the 11th and 1 hour on the 14th. This deviates markedly from typical auroral behaviour but is characteristic of NLC. The patch shows no ray structure and the sharp lower boundaries are not typical of auroral lower boundaries.

Kp values were 3^+ during the August 11 and 1 during the August 14 display. Figure 18 shows the statistical auroral oval at different degrees of magnetic activity (the Qp index is the hourly equivalent of the 3 hourly Kp index and for the purposes here, can be thought of as equivalent). The displays occurred at approximately 15^h L time. For Mawson's L latitude of 71° it can be estimated that for Kp = 3^+ auroras would probably be seen fairly low near the horizon in the southern sky. For Kp = 1 it is unlikely that auroras would be seen in any part of the sky. The probability at such Kp values of auroras being in the western sky is even lower.

NLC tend to appear over a period of a few days (Table 1) as these patches did. It is unlikely that unusual aurora would occur on days so close together, and in the morning and evening twilight sky, when the Kp is so low.

McDONALD (1964) has considered the relationships between total ambient pressure, saturation and actual water vapour pressure required for cloud formation. Figure 19 shows his exclusion limits for cloud formation based on the US Standard Atmosphere, together with the temperature - altitude profile of PETERSON et al (1966) taken over Kwajalein (9° 24' N). The inversion at 107 km is at about the level of the highest recorded mesopause inversions. For the luminous patch elevation of approximately 10° and SDA

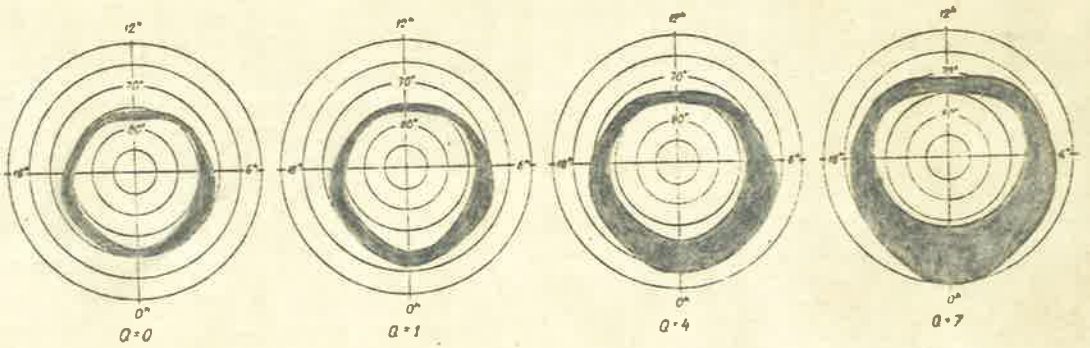

Fig. 18. The Auroral belt at different degrees of geomagnetic activity (after FELDSTEIN and STARKOV, 1965).

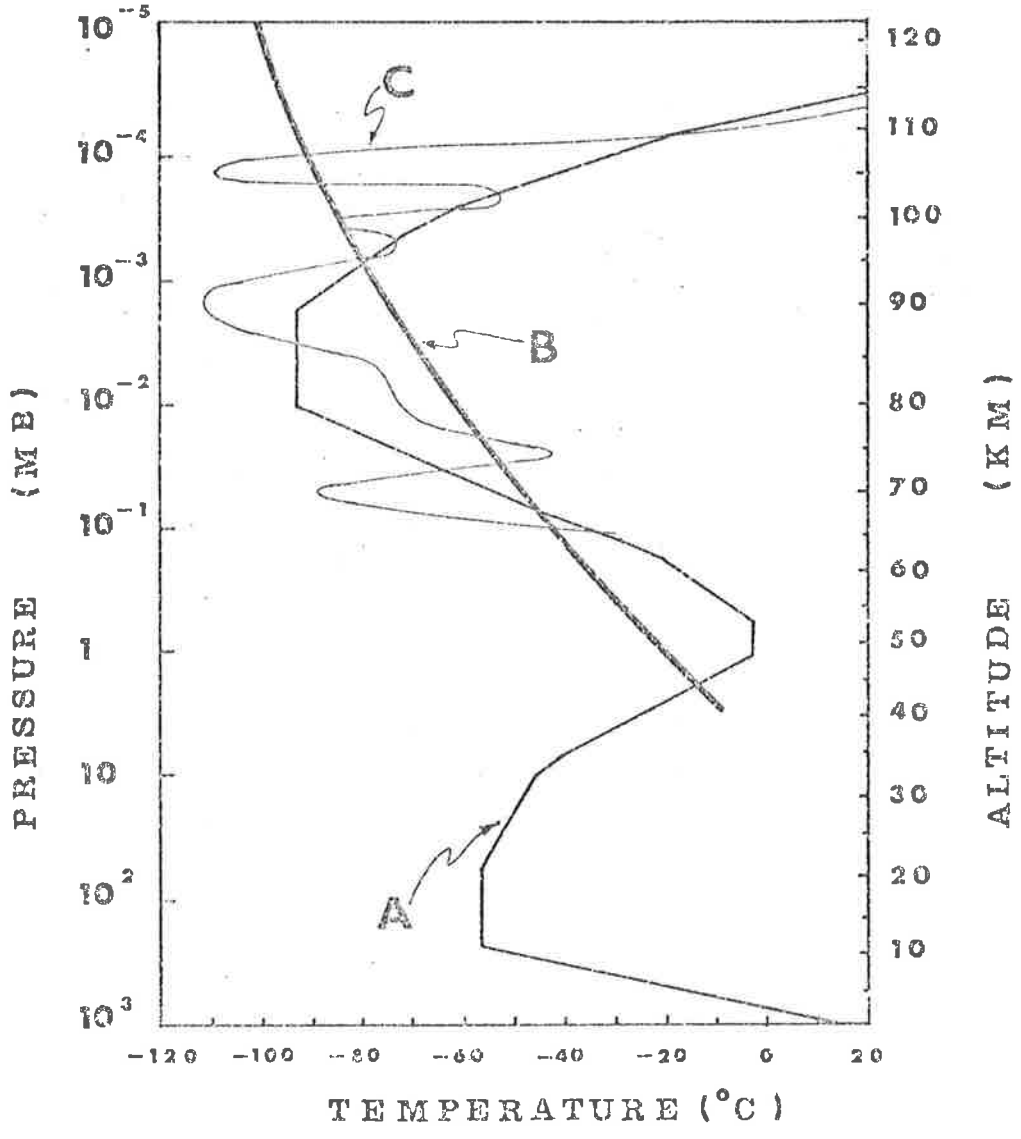

Fig. 19. Curve A is the 1962 U.S. Standard Atmosphere. Curve C is the temperature-height profile of PETERSON et al (1965). Curve B is the water cloud formation limit of McDONALD (1964). Water clouds cannot occur to the right of curve B.

of 16° and a screening height of 30 km, the earth's shadow height is about 138 km, indicating that the patches are at least that height. On the basis of Figure 19 it seems unlikely that ice clouds would occur at such a great height.

The above analysis has failed to settle the question of just what the patches were. The hypothesis that the patch was an aurora seems to be quite untenable. On the basis of McDonald's work, the hypothesis that the patch was an NLC would require that the temperature in the region of 138 km be abnormally low, especially for the month of August, in the Southern Hemisphere.

APPENDIX

PUBLICATIONS

JOURNAL OF GEOPHYSICAL RESEARCH VOL. 68, NO. 9 MAY 1, 1963

Letters

Behavior of Zenith [O I] 6300 A Airglow at Townsville during High-Altitude Nuclear Explosions

E. H. CARMAN, B. C. GIBSON-WILDE, B. P. KILFOYLE, AND W. M. COLEMAN

Department of Physics
University College of Townsville, Pimlico, Australia

Early reports of the high-altitude nuclear explosion over Johnston Island (169.5°W, 16.7°N) on July 9, 1962, show that the [O I] 6300 A airglow emission increased at places remote from the explosion. *Odencrantz et al.* [1962] observed an increase of the order of 10 rayleighs at China Lake, California (117.6°W, 35.7°N). F. E. Roach (private communication, 1962) has suggested that much higher increases of the order of hundreds of rayleighs might be expected in the magnetic conjugate region to Johnston Island. This prediction met with spectacular confirmation from New Zealand. The auroras observed there have been given wide publicity in both the daily and the popular scientific press (*Calder* [1962] for example). The expected enhancement should be centered very roughly where the meridian through Johnston Island intersects the approximate magnetic conjugate latitude, approximately in the neighborhood of Samoa (172°W, 14°S). The likelihood of a large increase occurring diminishes as the longitudinal distance to the east or west becomes greater. It is of considerable importance to delineate the conjugate region, and in this connection it might be expected that the east coast of Australia in the vicinity of, say, Townsville (latitude 19.25°S, longitude 146.75°E, and geomagnetic latitude 28.4°S) would be an interesting point at which to observe the western limits of this conjugate region. This note is written with that purpose in mind.

Results of a preliminary examination of measurements carried out at Townsville for the high-altitude explosions of July 9, October 20, October 26, November 1, and November 4, 1962, appear in Figure 1. The plots represent diurnal zenith values determined by means of a photometer [*Huruhata et al.*, 1957] fitted with an interference filter centered near 6300 A. The values shown are approximate rayleighs pending accurate calibration of the reference source of the photometer. They are reduced from actual observations made at 16-minute intervals throughout the hours of darkness on the five nights mentioned above. The approximate zero times shown on the plots were obtained by monitoring the countdown broadcast from Johnston Island. The reported approximate yield of the July explosion was one megaton, that of October 26 one hundred kilotons, and the rest were of the order of tens of kilotons.

Significantly, large increases in intensity are evident on the nights of October 26/27 and November 1/2 and 4/5, but it is not likely that these increases result solely from the ionization effects of the nuclear explosions. *Very similar behavior has been observed on other nights during October on which no high-altitude nuclear explosion was reported.* Further evidence that the 6300 A emission was not markedly increased over Townsville is apparent from Figure 2, in which the maximum middle of the night values from diurnal curves for 23 nights during the period of the tests are plotted. Enhanced twilight values have been disregarded; the plotted maximums occur during the local time period 2230 to 0330 h. These plots show that red airglow increases progressively as summer is approached. It will be noted that the values corresponding to the five nuclear test nights conform to this general pattern, suggesting that the enhancements on those nights are due to seasonal trends rather than the effects of nuclear explosions. Middle of the night enhancement similar to that shown in the diurnals of Figure 1 has

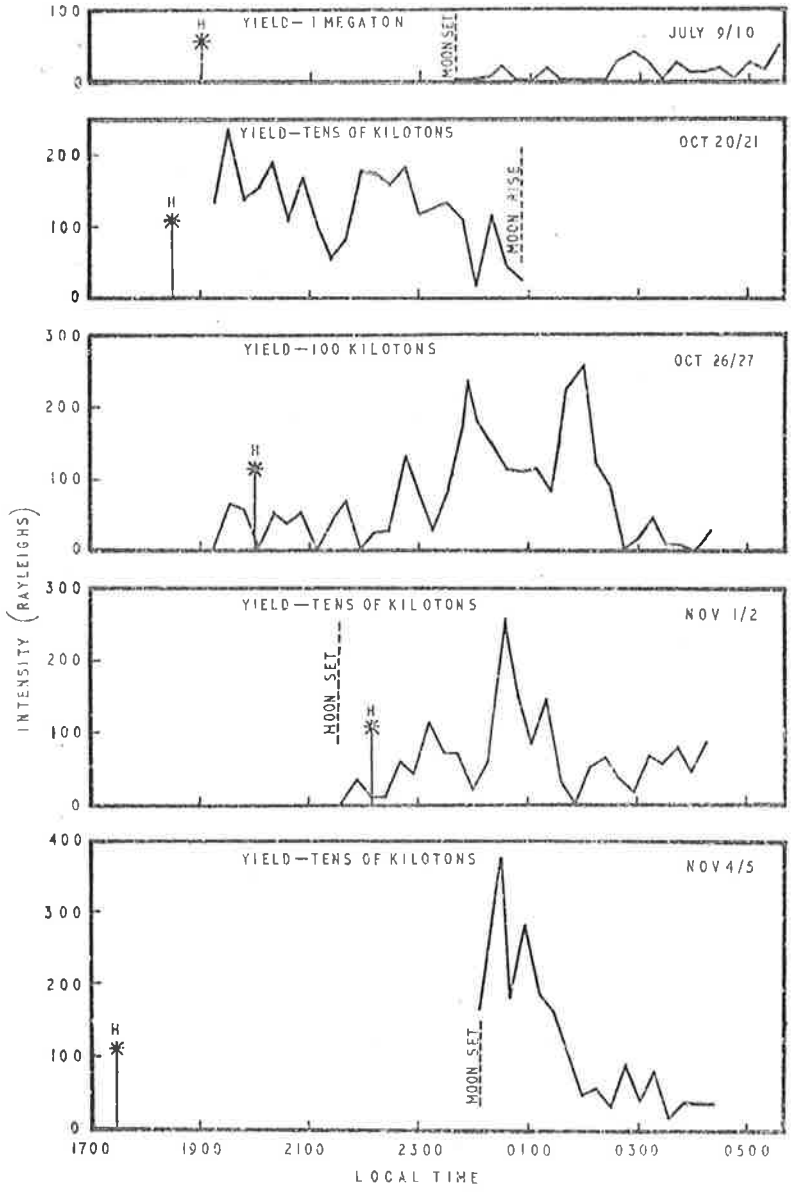

Fig. 1. Diurnal variation of [O I] 6300 A airglow on five nights of high-altitude nuclear explosions. The approximate zero times are marked by the letter *H*.

been observed at Maui [*Barbier et al.*, 1962] which is roughly magnetically conjugate to Townsville. This behavior was observed on summer nights, suggesting further that midnight or early morning enhancement is to be expected at least during summer in tropical latitudes.

It is possible of course that small increases in red airglow, of the kind found by Odencrantz et al., did occur over Townsville after the explosions. As mentioned by those authors, such small increases could be accounted for by pair production resulting from electromagnetic radiation or neutron beams, and thus the effect is of short duration, lasting only some 150 seconds after the explosion. Unfortunately there are no quantitative zenith measurements available at Townsville for the July 9 explosion. The only two nights on which quantitative observations were actually in progress at the time of a high-altitude nuclear explosion are October 26/27 and No-

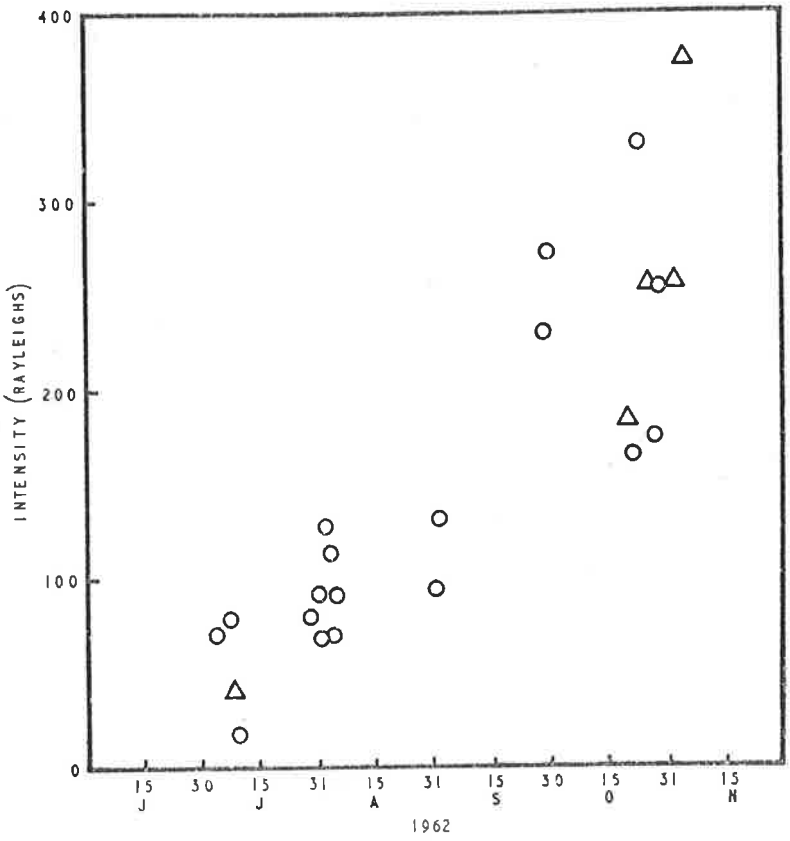

Fig. 2. Maximum values of intensity for various nights throughout the test season. Triangles represent values obtained on nights of nuclear explosion; circles represent values obtained on nights when no explosion was reported.

vember 1/2. Variation in zenith airglow in the approximate interval 200 seconds before and 300 seconds after zero time is shown in Figure 3. The variations shown there are of the same order as the random fluctuations due to the relative accuracy of scaling of the recording chart, approximately ±25 rayleighs. Therefore it must be concluded that the present method of observation might not be sufficiently sensitive to detect small increments of the order of 10 rayleighs unambiguously.

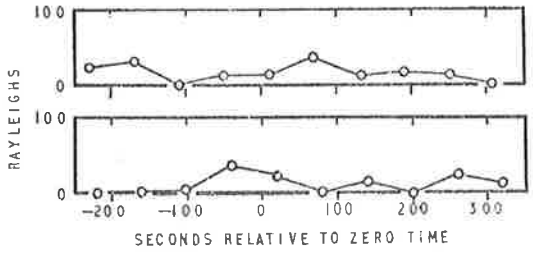

Fig. 3. Variation of airglow near zero time. The fluctuations shown are due mainly to experimental error.

A complete analysis of all observations at Townsville during the test period, including ionosonde data, is being prepared for publication.

References

Barbier, D., F. E. Roach, and W. R. Steiger, The summer intensity variations of [O I] 6300 A in the tropics, *J. Res. NBS, 66D*, 145, 1962.

Calder, N., Effects of the space bomb, *New Scientist, 15*, 72, 1962.

Huruhata, M., T. Nakamura, and H. Tanabe, Scanning photoelectric photometer and method of observation of night airglow for the international geophysical year, *Tokyo Astron. Bull.*, [2]*94*, 1005, 1957.

Odencrantz, F. K., P. Saint-Amand, and J. G. Moore, Zenith airglow observations during the high-altitude nuclear explosion of July 9, 1962, *J. Geophys. Res., 67*, 4091–4092, 1962.

(Received January 9, 1963.)

Carman, E. H., Gibson-Wilde, B. C., Kilfoyle, B. P., & Coleman, W. M. (1963). Tropical Twilight Behaviour of the [01] 6300 Å Air Glow at Townsville. *Nature, 198,* 1077

JOURNAL OF GEOPHYSICAL RESEARCH VOL. 68, NO. 19 OCTOBER 1, 1963

Letters

Relationship between [O I] 6300 A Zenith Airglow and Ionospheric Parameters f_oF_2 and $h'F$ at Townsville

E. H. CARMAN AND B. P. KILFOYLE

Department of Physics
University College of Townsville, Townsville, Australia

Barbier et al. [1962] found striking agreement between photometer measurements of the [O I] 6300 A night airglow and calculated values based on the ionospheric parameters f_oF_2 and $h'F$. The published observations were made in the northern tropics at Maui (latitude 20.8°N, longitude 156.5°W) on three summer nights during 1961. The comparison was between observed values and values calculated according to *Barbier's* [1957] semiempirical formula:

$$Q = A(f_oF_2)^2 \exp\left(-\frac{h'F - 200}{H}\right) + C$$

where Q is the intensity in rayleighs, H is the scale height, and A and C are constants. *Barbier et al.* [1962] assumed $H = 41.3$, and for the constants they derived the values $A = 3.84$, $C = 18$. At Tamanrasset *Barbier and Glaume* [1962] found the values $A = 2.94 \pm 0.12$ and $C = 109 \pm 4.2$. These results were obtained from a statistical calculation based on the accumulated values of airglow and ionospheric parameters observed in the three-year period between May 1957 and November 1960. There were insufficient data from any one night, however, to directly compare observed with calculated values from the Tamanrasset observations.

In the present note, observed variation of red airglow is compared with the variation calculated according to a simplified form of Barbier's relation for three representative nights during the winter, spring, and summer of 1962 in the southern tropics at Townsville (latitude 19.25°S, longitude 146.75°E, geomagnetic latitude 28.4° S). For convenience in making a comparison, the constant C has been ignored and A has been given an arbitrary value to bring calculated and theoretical curves for each night into coincidence at the maximum middle-of-the-night value.

The photometer [*Huruhata et al.*, 1957] employed in the observations is fitted with two interference filters centered on 6300 A and 5300 A. The 5300 A filter serves to eliminate zodiacal background. This instrument was operated on the same site as the vertical incidence sounder of the Townsville Ionospheric Prediction Station. Simultaneous observations of zenith airglow intensity and ionospheric parameters were possible, since the intensity was recorded at one-minute intervals and the parameters at fifteen-minute intervals.

Figure 1 shows the general trend for the five months covered by the observations. The observed values are approximate pending accurate calibration of the reference source of the photometer. The June 3–4 results are characteristic of winter quiescent conditions at Townsville. On the other hand, the curves for November 4–5 show enhanced behavior after midnight similar to that found by *Barbier et al.* [1962] at Maui for summer nights. Behavior intermediate between these two extremes is apparent from the results for August 1–2. On all three nights the same excellent agreement between the observed and calculated values is obtained as at Maui.

The red airglow intensity in the approximate interval between midnight and 0300 local time shows a marked seasonal increase as summer is approached. In addition to the Figure 1 results, the same tendency for red airglow to increase with the approach of summer has been observed on twenty other nights investigated during the five months by several people [*Carman et al.*, 1963].

From a graphical comparison of the actual parameters $h'F$ and f_oF_2, *Barbier et al.* [1962] concluded that $h'F$ was the dominating factor for 6300 A emission at Maui. An analysis of the

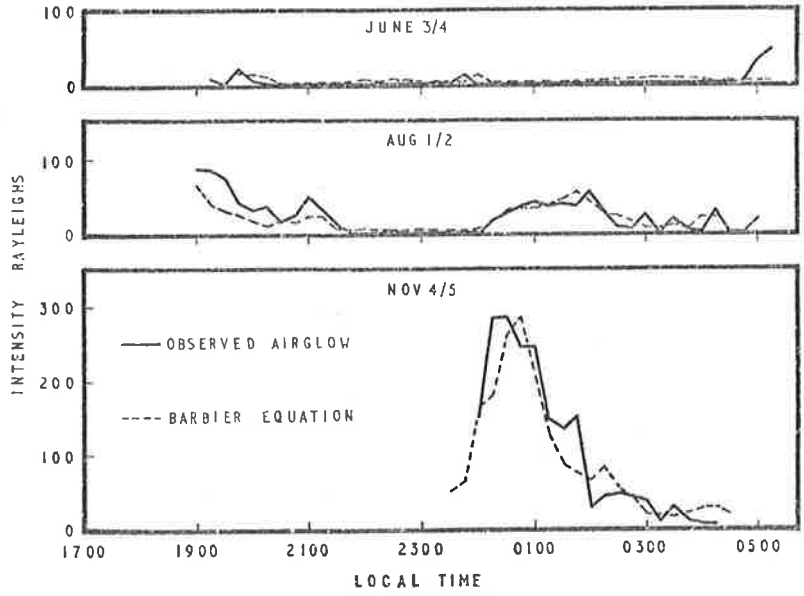

Fig. 1. Comparison between observed zenith airglow and values calculated according to Barbier's relation based on ionospheric observations. The three sets of curves show typical seasonal variations at Townsville.

relative contributions of the ionospheric parameters for Townsville is given in Figure 2. Here observed airglow in rayleighs is plotted on the same graph as the functions $(f_0F_2)^2$ and exp $[-(h'F - 200)/41.3]$. These two functions are plotted on an arbitrary scale with the maximum values normalized to the maximum middle-of-the-night observed airglow as in Figure 1.

Although the constituent functions vary in form, the graphs show that they contribute roughly equally to the resultant calculated airglow. For the night of August 1–2 exp $[-(h'F - 200)/41.3]$ has the better correlation up to 0300 LT; it then diverges markedly from the observed airglow. On the other hand, the curves for November 4–5 indicate better correlation between $(f_0F_2)^2$ and observed airglow for all times during the night.

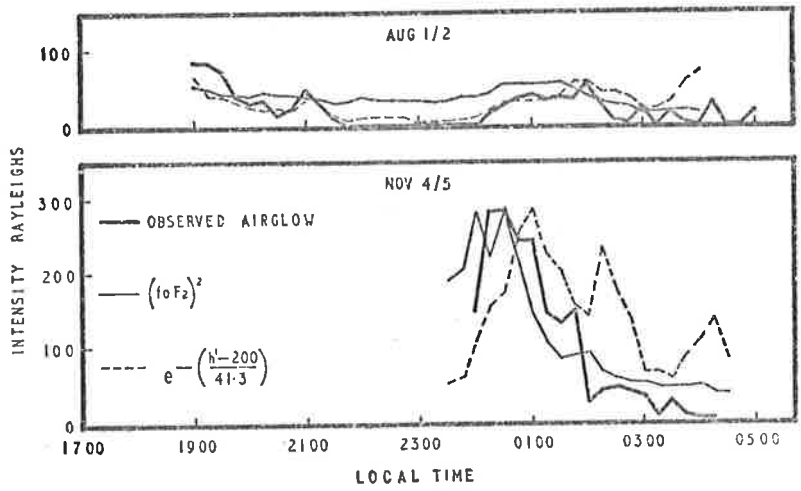

Fig. 2. Relative agreement of observed airglow with functions involving the ionospheric parameters f_0F_2 and $h'F$.

Further airglow-ionospheric parameter correlation from the present series of observations is being prepared for publication.

Acknowledgment. We are indebted to the Commonwealth Ionospheric Prediction Service and the Officer in Charge of the Townsville Station, A. B. D. Drury, for providing data before publication.

References

Barbier, D., La lumière du ciel nocturne en été a Tamanrasset, *Compt. Rend., 245,* 1559–1561, 1957.

Barbier, D., and J. Glaume, La couche ionosphérique nocturne *F* dans la zone intertropicale et ses relations avec l'emission de la raie 6300 A du ciel nocturne, *Planetary Space Sci., 9,* 133–148, 1962.

Barbier, D., F. E. Roach, and W. R. Steiger, The summer intensity variation of [O I] 6300 A in the tropics, *J. Res. NBS, 66D*(1), 145–152, March–April 1962.

Carman, E. H., B. C. Gibson-Wilde, B. P. Kilfoyle, and W. M. Coleman, Behavior of zenith [O I] 6300 A air glow at Townsville during high-altitude nuclear explosions, in press, 1963.

Huruhata, M., T. Nakamura, and H. Tanabe, Scanning photoelectric photometer and method of observation of night airglow for the International Geophysical Year, *Tokyo Astron. Bull., 2nd Ser.,* no. 94, 1005, 1957.

(Received June 21, 1963.)

JOURNAL OF GEOPHYSICAL RESEARCH VOL. 69, NO 21 NOVEMBER 1, 1964

Pattern of the [O I] 6300 A Airglow Emitting Regions at Townsville

E. H. CARMAN, B. P. KILFOYLE, AND B. C. GIBSON-WILDE

Department of Physics
University College of Townsville, Queensland, Australia

The size and brightness of the airglow emitting regions investigated at Townsville (latitude, 19.25°S; longitude, 146.75°E; geomagnetic latitude, 28.4°S) during the period between July and November 1962 undergo systematic diurnal and seasonal changes. Diurnal behavior in the tropical zone is characterized by middle-of-the-night enhancement on some summer nights. Enhanced 6300 A airglow from regions 500 to 1000 km in diameter centered on a single sky location were observed by *Barbier et al.* [1962] at Maui (latitude, 20.8°N; longitude, 156.5°W; geomagnetic latitude, ~20°) in the northern summer of 1964. This kind of behavior also occurs at Townsville; it has been established there [*Carman and Gibson-Wilde,* 1964] that early summer middle-of-the-night enhancement develops progressively from complete absence in winter. In this letter the diurnal and seasonal variations of the emission pattern are studied in detail for a typical winter and a typical early summer night.

The photometer [*Hirahata et al.,* 1957] employed in the present observations completes one scan of the sky every 16 minutes in steps of 1 minute corresponding to 16 equally spaced azimuth directions. During each azimuth interval the instrument observes in the six zenith directions given in Table 1. The second column in the table shows the approximate radius of the circular area swept out in the emitting layer, assuming a height of about 250 km. The photometer is fitted with narrow band interference filters centered on 6300 A and 5300 A, the latter to measure zodiacal and stellar sky background.

Figures 1 and 2 show complete sets of diurnal curves representing the intensity variation for typical winter quiescent and spring enhanced conditions along the N-S and E-W directions. The data of Figure 2 for the night of Nov. 4–5 are also included in Figure 3, which shows all data for the night plotted as sixteen isophote sky maps. These maps give values of intensity in approximate rayleighs measured as described in the last paragraphs for sixteen consecutive scans of the photometer. Individual maps represent the average pattern of emission intensity during the respective sixteen-minute scanning periods. The maps of Figure 3 are only rough approximations to the corresponding series of instantaneous patterns, because the marked progressive changes which obviously do occur, particularly between midnight and 0100 hours, coincide with the progressive sweep of the photometer as it moves counterclockwise. This results in a sixteen-minute lag between the first and last azimuthal positions observed for each map, and considerable distortion is inevitable. This restriction applies to a lesser extent when the pattern is more or less stable, as between 0300 and 0400 hours. On the other hand, the over-all behavior throughout the observed part of the night is fairly well represented by the complete set of maps. This suggests a more accurate picture of the size of emitting regions might result from a method involving a comparison of the variation of intensity at various points as the night progresses rather than by measurement from individual sky maps. *Roach et al.* [1958] have devised such a method for determining the size of emitting regions for [O I] 5577 A airglow. This method of comparing diurnal changes is based on the assumption that regions associated with the same element of airglow emitting pattern tend to produce parallel diurnal variations. For example, the

TABLE 1

Zenith Angle θ	Scanning Radius, km
38°42′	160
53°6′	320
63°24′	480
69°24′	640
73°18′	800

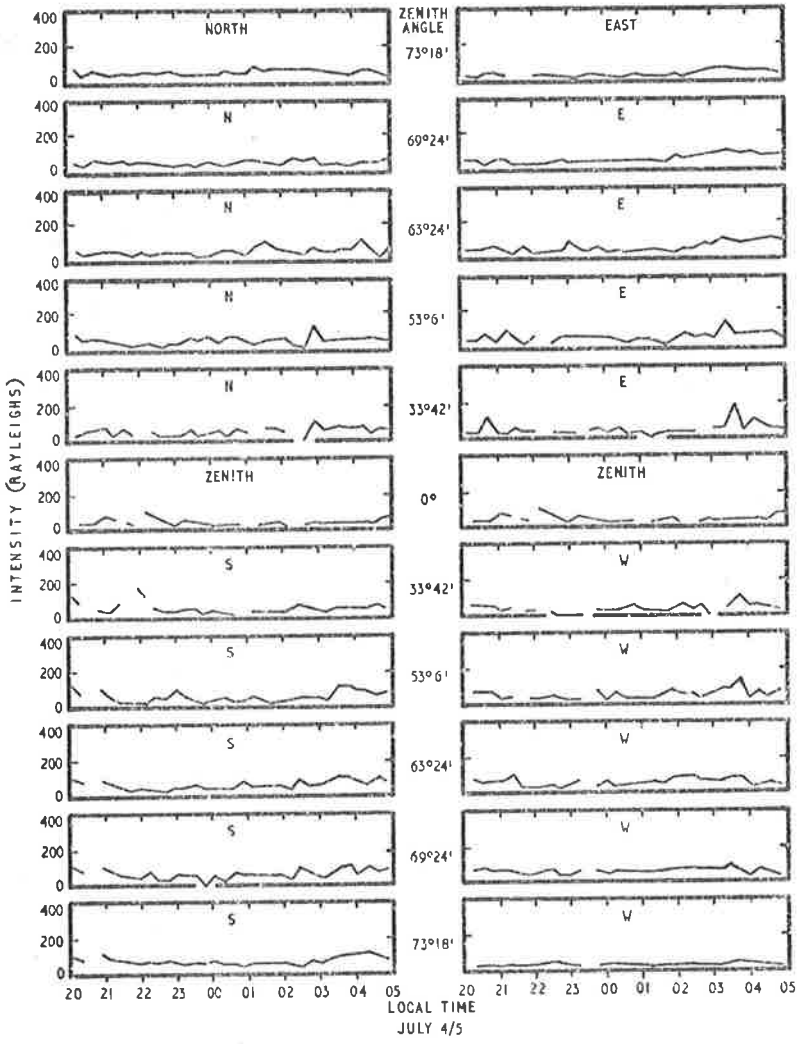

Fig. 1. Red airglow diurnal curves for a typical winter night. The curves represent values in the N-S and E-W directions.

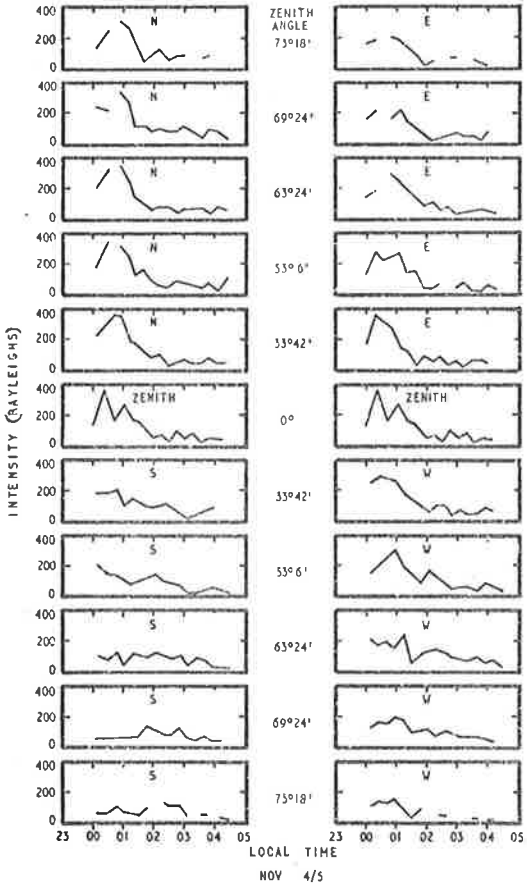

Fig. 2. Red airglow diurnal curves for a typical early summer night on which anomalous after-midnight enhancement occurs.

northern parts of the sky, represented by the six diurnal curves from zenith to 73°18′N in Figure 2, undergo similar changes and therefore ought to correspond to the same emitting region. The same can be said for most of the E-W diurnal curves. Correlation between points on the respective diurnal curves is to be expected, therefore, and in the present work the rank difference coefficient

$$p = 1 - [6\Sigma d^2/n^2(n - 1)] \qquad (1)$$

employed by *Roach et al.* [1958] is used. In this relation d is the difference of rank between pairs of points corresponding to the same time, and n is the total number of such pairs of readings.

In applying the technique to the present observations, the two orthogonal sets of data appearing in Figure 2 are analyzed to obtain eleven values of p in each of the two directions. In the N-S direction for each time of the night the value of intensity at 73°18′N is compared with the corresponding values for the remaining 10 zenith distances. In the E-W the comparison is between the 73°18′W and the remainder.

When the diurnal intensity is relatively low, say less than about 100 rayleighs, the random variations take control, and it is not possible to speak of parallel diurnal variations. This is the case for the southern sky on Nov. 4–5, and for the whole sky on July 4–5 (Figures 1 and 2). Thus equation 1 will only have significance when applied to a night of enhanced emission, as in Figure 2. Figure 4 shows the correlation coefficient as a function of distance from the respective reference points for both N-S and E-W directions for Nov. 4–5. For p to have significance in terms of the geometric magnitude of single airglow emission features, it must be greater than $2/(n - 3)^{1/2}$, i.e. greater than 0.60 in the present case [*Roach et al.*, 1958]. According to Figure 4, this corresponds roughly to linear dimensions of the order of 1000 km.

It will be clear from the preceding paragraphs that the correlation coefficient method will not yield useful results for the quiescent winter conditions of July 4–5. A comparison of Figures 1 and 2 shows that the all-night behavior of July 4–5 is similar to the behavior on November 4–5 in all observed positions of the sky during the last hour or so before dawn. It follows that the emission pattern throughout the whole night of July 4–5 will be similar to the almost uniform regions illustrated in the last four isophotes of Figure 3. With this simple picture for winter representing one extreme during the observed season and the early summer behavior of November 4–5 corresponding to the other extreme, the over-all behavior for the season can be summarized as follows. In winter there is no tendency for a systematic anomalous pattern to develop, either at twilight [*Carman et al.*, 1963] or throughout the night. Twilight enhancement of the order of 200 rayleighs is followed by a general decrease to less than 50 rayleighs. Early summer behavior falls into two classes, quiescent and enhanced nights. Quiescent nights are characterized by absence of anomalous middle-of-the-night enhancement

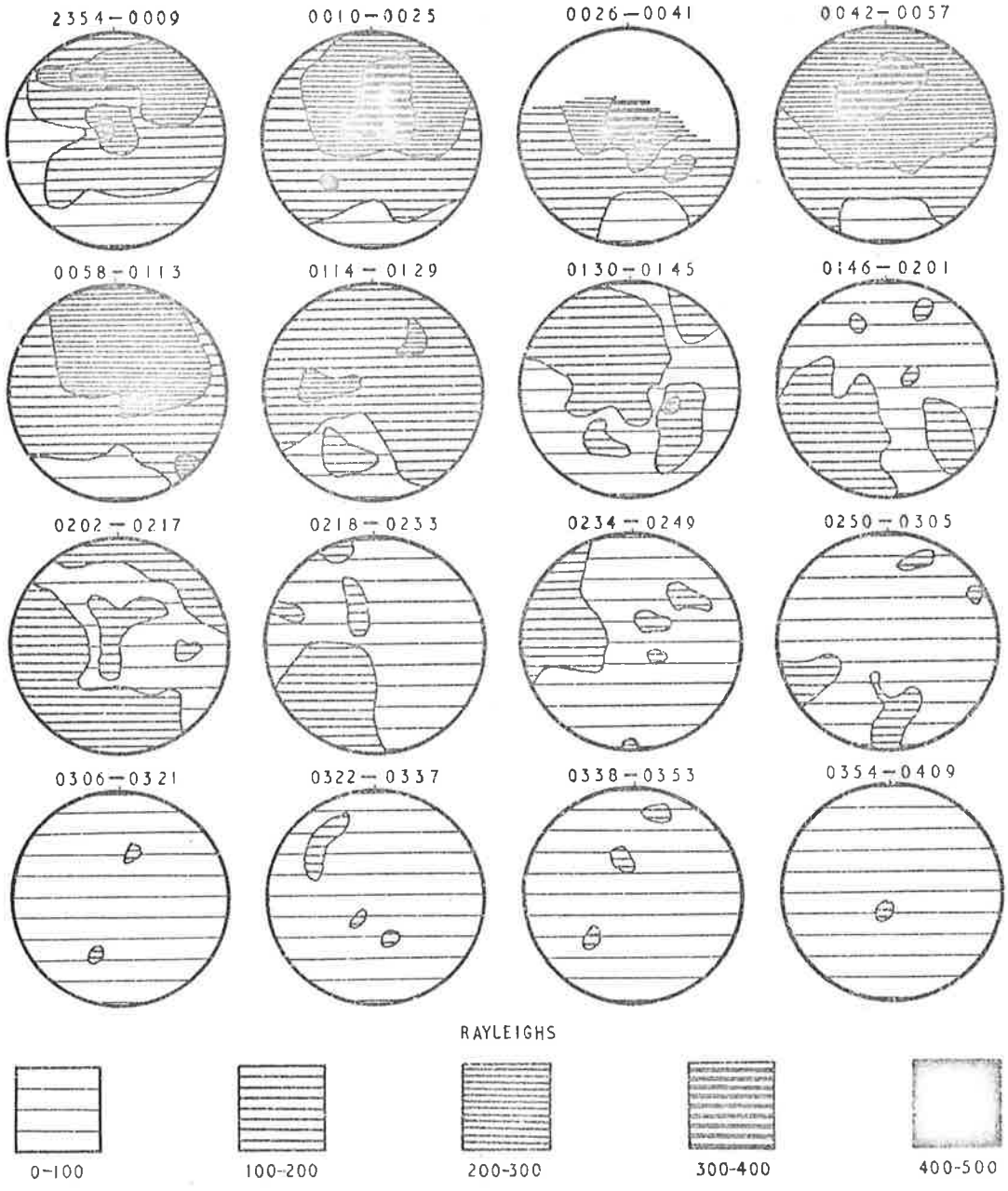

Fig. 3. Isophote sky maps of the red airglow emissions represented in Figure 2. Each map corresponds to observations made during a complete sweep of the photometer. The local time at the beginning and end of each sweep is given at the top of each map.

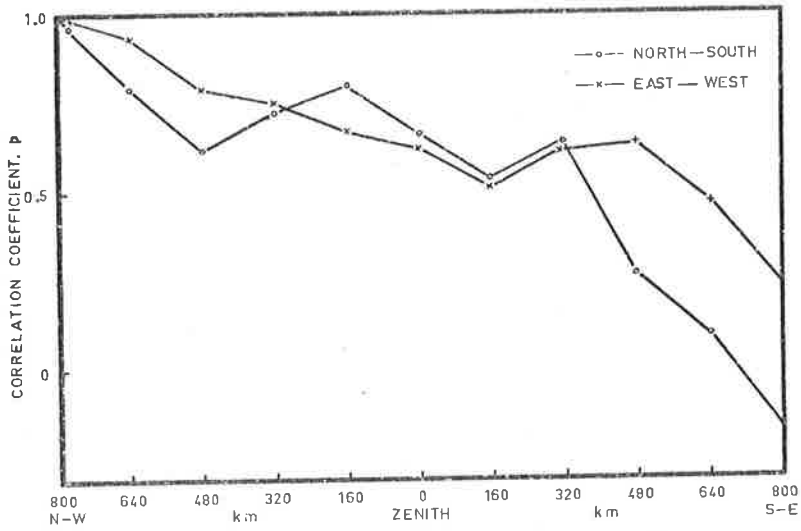

Fig. 4. Variation of the rank difference coefficient with position. The correlation is made between points across the emitting region referred to locations in the emitting layer at zenith angles 73°18′ in north and west.

of the kind shown in the northern sky in Figure 3, but they tend to show an anomalous twilight enhancement in the south-southwest [cf. *Barbier*, 1961, 'La nappe occidentale']. Enhanced early summer nights seem to have a two-fold behavior: the sky can be resolved into large regions of low intensity (less than 200 rayleighs) on which are superimposed cloud-like features of rapidly varying intensity measuring up to about 1000 km in diameter. These airglow 'clouds' exist mainly in the equatorial zone to the north of the Townsville latitude.

Studies of the ionospheric parameters f_0F_2 and $h'F$ indicate that the airglow clouds have their origin in an increase in electron density accompanied by a reduction in the base height of the F layer. The diurnal variation in this connection has been described by *Carman and Kilfoyle* [1963] and latitude effects by *Carman* [1964]. An investigation of the seasonal aspects of the latitude correlation between ionospheric parameter and enhanced red airglow is proceeding.

Acknowledgment. We are indebted to our colleague, Mr. Leon Offenhauser, for his assistance in the preparation of the paper.

References

Barbier, D., Les variations d'intensité de la raie 6300 A de la luminescence nocturne, *Ann. Geophys., 17*, 3–15, 1961.

Barbier, D., F. E. Roach, and W. R. Steiger, The summer intensity variations of [O I] 6300 A in the tropics, *J. Res. NBS, 66D*, 145, 1962.

Carman, E. H., Dependence of [O I] 6300 A airglow on latitude as observed from Townsville, Australia, *Nature, 201*, 595–596, February 8, 1964.

Carman, E. H., and B. C. Gibson-Wilde, Seasonal variation of the [O I] 6300 A airglow at Townsville from isophote sky maps, *J. Geophys. Res., 69*(3), 487, 1964.

Carman, E. H., B. C. Gibson-Wilde, B. P. Kilfoyle, and W. M. Coleman, Tropical twilight behavior of the [O I] 6300 A airglow at Townsville, *Nature, 198*, 1077–1078, June 15, 1963.

Carman, E. H., and B. P. Kilfoyle, Relationship between [O I] 6300 A zenith airglow and ionospheric parameters for f_0F_2 and $h'F$ at Townsville, *J. Geophys. Res., 68*(18), 5605, 1963.

Huruhata, M., T. Nakumura, and H. Tanabe, Scanning photoelectric photometer and method of observation of night airglow for the International Geophysical Year, *Tokyo Astron. Bull., 2*, 94 and 1005, 1957.

Roach, F. E., E. Tandberg-Hanssen, and L. R. Megill, The characteristic size of airglow cells, *J. Atmospheric Terrest. Phys., 13*, 113–121, 1958.

(Manuscript received June 29, 1964.)

Kilfoyle, B. P. (1968). Antarctic Sightings of Noctilucent and Nacreous Clouds. *Nature, 218,* 154.

Kilfoyle, B. P., & Jacka, F. (1968). Geomagnetic L Coordinates. *Nature*, *220*, (5169) 773-775.

ACKNOWLEDGMENTS

This investigation was carried out for the Antarctic Division, Department of Supply, and the assistance of members of that organisation is gratefully acknowledged, especially that of Mr. P.H. Sulzberger, the Acting Assistant Director (Scientific) and of Major F.R. Bond, who gave much advice and assistance.

The observations were made while the author was a member of the 1966 Australian National Antarctic Research Expeditions. The equipment used was designed and constructed by the Antarctic Division. The author's role was to maintain the equipment, continue certain research programs and to initiate new research. The valuable electronic assistance of Mr. A. Williams is gratefully acknowledged.

The analysis of the data was carried out at the Mawson Institute for Antarctic Research, and the author is indebted to the Director of the Antarctic Division for continuing his salary for part of the time he was engaged there.

The author is further indebted to the Director of the Mawson Institute for Antarctic Research, Dr. F. Jacka, for guidance and helpful criticism throughout this investigation.

The cooperation of the Officers in Charge of the Geophysical Observatories at Kiruna and Murmansk in supplying data is acknowledged.

The typing and general assistance of Miss K. Palmer in the preparation of the thesis is gratefully acknowledged.

REFERENCES

AKASOFU, S.-I. (1964) Plan. Space Sci. 12, 273.

AKASOFU, S.-I. (1968) "Polar and Magnetospheric Substorms", D. Reidel Publishing Company, Dordtrecht, Holland.

ANSARI, Z.A. (1965) J. Geophys. Res. 70, 3117.

BAILEY, D.K. (1968) Rev. Geophys. 6, 289.

BERKEY, F.T. (1968) J. Geophys. Res. 73, 319.

BEWERSDORFF, A., KREMSER, G., RIEDLER, W., and LEGRAND, J.P. (1967) Arkiv. Geofysik. 5, 115.

BEWERSDORFF, A., KREMSER, G., STADSNESS, J., TREFALL, H. and ULLALAND, S. (1968) J. Atmosph. Terr. Phys. 30, 591.

BOND, F.R. (1968) Ann. Geophys. 24, 1.

BROWN, R.R. (1964) J. Geophys. Res. 69, 2315.

CAMPBELL, W.H. and MATSUSHITA, S. (1967) J. Geophys. Res. 72, 3518.

CHAMBERLAIN, J.W. (1961) "Physics of the Aurora and Airglow". Academic Press, New York.

COLE, K.D. (1963) Aust. J. Phys. 16, 423.

EATHER, R.H. (1968) J. Geophys. Res. 73, 119.

EATHER, R.H., and JACKA, F. (1966a) Aust. J. Phys. 19, 215.

EATHER, R.H., and JACKA, F. (1966b) Aust. J. Phys. 19, 241.

EATHER, R.H. and SANDFORD, B.P. (1966) Aust. J. Phys. 19, 25.

FEDYAKINA, N.I. (1963) Geomagnetizm I Aeronomiya 3, 393.

FELDSTEIN, Y.I., and STARKOV, G.V. (1967) Plan. Space Sci. 15, 2, 209.

FOGLE, B. (1964) Geophysical Institute Rep. No. UAG R-158, Univ. Alaska.

FOGLE, B. (1965) Nature 207, 66.

FOGLE, B. (1966) Geophysical Institute Rep. No. UAG R-177, Univ. Alaska.

FOGLE, B. and HAURWITZ, B. (1966) Space, Sci. Rev. 6, 279.

GORDON-SMITH, G.W. (1952) Proc. Roy. Soc. B 65, 275.

FRANCIS, R.J., BENNETT, J.M. and SEEDSMAN, D.L. (1966) Nature 211, 398.

FRANCIS, R.J. (1967) M.Sc. Thesis, Univ. Adelaide.

FRANCIS, R.J. and JACKA, F. (1969) J. Atmosph. Terr. Phys. 31, 321.

HAKURA, Y. (1965) Rep. Ionosph. Space Res. Japan 19, 121.

HAMILTON, R.A. (1964) Met. Mag. 93, 201.

HARGREAVES, J.K. and COWLEY, F.C. (1967) Plan. Space Sci. 15, 1571.

HARTZ, T.R., MONTBRIAND, L.E., and VOGAN, E.L. (1963) Canad. J. Phys. 41, 581.

HOOK, J.L. (1968) J. Atmosph. Terr. Phys. 30, 1341.

HULTQVIST, B. (1958) Arkiv. Geofys. 3, 63.

JELLY, D. and BRICE, N. (1967) J. Geophys. Res. 72, 5919.

KILFOYLE, B.P. (1968) Nature 218, 154.

KILFOYLE, B.P. and JACKA, F. (1968) Nature 220, 773.

LITTLE, C.G. and LEINBACH, H. (1959) Proc. Inst. Radio Engrs. 47, 315.

McDONALD, J.E. (1964) J. Geophys. Res. 69, 3669.

McILWAIN, C.E. (1961) J. Geophys. Res. 66, 3681.

MIDDLETON, W.E.K., and SAUNDERS, C.L. (1951) J. Opt. Soc. Am. 41, 419.

MONTBRIAND, L.E., TINSLEY, B.A. and VALLANCE-JONES, A. (1955) Canad. J. Phys. 43, 782.

PETERSON, J.W., HANSEN, W.H., McWATTERS, K.D. and BONFANTI, G. (1965) J. Geophys. Res. 70, 4477.

RODGERS, A.W., CAMPBELL, C.T., WHITEOAK, J.B., BAILEY, H.H. and HUNT, V.O. (1960) "An Atlas of H-Alpha Emission In The Southern Milky Way", Mt. Stromlo Observatory, Aust. Nat. Univ.

RODMAN, J.P. and SMITH, J. (1963) Applied Optics 2, 181.

SANDFORD, B.P. (1964) *J. Atmosph. Terr. Phys.* 26, 749.

SANDFORD, B.P. (1968) *J. Atmosph. Terr. Phys.* 30, 1921.

SIMINOW, G.V. (1963) *Geophys. J. R.A.S.* 8, 258.

STORMER, C. (1955) *"The Polar Aurora", Clarendon Press, Oxford.*

VEGARD, L. (1912) *Phil. Mag.* 23, 211.

VEGARD, L. (1932) *Norske Videnskapsakademi Geofysiske Publikajoner* 9, 11, 51.

VEISSBERG, O.L. (1962) *Aurora and Airglow* 8, 36.

——— (1963) *"International Auroral Atlas", Published by the International Union of Geodesy and Geophysics, Univ. of Edinburgh Press.*